Pseudo-Monthly Raman Lidar Dataset for Reference Water Vapor Observations in the UTLS

Dunya Alraddawi, Philippe Keckhut, Guillaume Payen, Jean-Luc Baray, Florian Mandija, Abdanour Irbah, Alain Sarkissian, Michael Sicard, Alain Hauchecorne, Hélène Vérèmes

remote sensing

MDPI

Article

Pseudo-Monthly Raman Lidar Dataset for Reference Water Vapor Observations in the UTLS

Dunya Alraddawi [1,*], Philippe Keckhut [1], Guillaume Payen [2], Jean-Luc Baray [3,4], Florian Mandija [1], Abdanour Irbah [1], Alain Sarkissian [1], Michael Sicard [5,6], Alain Hauchecorne [1] and Hélène Vérèmes [5]

1 Laboratoire Atmosphere et Observations Spatiales LAT MOS/Institut Pierre Simon Laplace IPSL, UVSQ Université Paris-Saclay, Sorbonne Université, Centre National de Research Sscientifique CNRS, 78280 Guyancourt, France; philippe.keckhut@latmos.ipsl.fr (P.K.); florian.mandija@latmos.ipsl.fr (F.M.); abdenour.irbah@latmos.ipsl.fr (A.I.); alain.sarkissian@latmos.ipsl.fr (A.S.); alain.hauchecorne@latmos.ipsl.fr (A.H.)
2 Observatoire des Sciences de l'Univers de La Réunion (OSU-Réunion), UAR 3365, Université de La Réunion, Centre National de Recherche Sscientifique CNRS, Météo-France, IRD, 97400 Saint-Denis, France; guillaume.payen@univ-reunion.fr
3 Observatoire de Physique de Globe de Clermont OPGC, UAR 833, Centre National de Recherche Sscientifique CNRS, Université Clermont Auvergne, 63100 Clermont-Ferrand, France; j.l.baray@opgc.fr
4 Laboratoire de Météorologie Physique LaMP, UMR 6016, Centre National de Recherche Sscientifique CNRS, Université Clermont Auvergne, 63100 Clermont-Ferrand, France
5 Laboratoire de l'Atmosphère et des Cyclones (LACy), Météo-France, Université de la Réunion, Centre National de Recherche Sscientifique CNRS, 97744 Saint Denis, France; michael.sicard@univ-reunion.fr (M.S.); helene.veremes@univ-reunion.fr (H.V.)
6 Department of Signal Theory and Communications, Universitat Politècnica de Catalunya, 08034 Barcelona, Spain
* Correspondence: dunya.alraddawi@latmos.ipsl.fr

Highlights

A new approach using pseudo-monthly lidar averages has enabled the evaluation of water vapor mixing ratios (WVMR) up to subtropical upper tropospheric altitudes. This dataset now spans over 11 years of humidity profiles and can be compared with data from MLS-Aura, ERA5, and GRUAN-analyzed radiosondes. Both MLS and GRUAN analyses show systematically drier values relative to the lidar, particularly above 12 km, whereas ERA5 values exhibit better agreement. These findings suggest that calibrating lidar WVMR using ERA5 could serve as a viable alternative to improve lidar estimates in the upper troposphere.

What are the main findings?

- MLS and GRUAN-analyzed M10 radiosondes consistently exhibit drier values compared to lidar observations in the upper troposphere over Réunion Island.
- The current lidar data processing aligns more closely with ERA5 reanalysis data in the subtropical upper troposphere.
- An alternative lidar calibration increases WVMR in the upper troposphere.

What are the implications of the main findings?

- Enhancing the quality of Raman lidar water vapor observations and improving their consistency with radiosonde measurements in the upper troposphere/lower stratosphere (UTLS).
- Improving satellites and reanalysis observations over the subtropical upper troposphere.

Academic Editors: Shengyang Gu, Haiyang Gao and Zhaoai Yan

Received: 12 February 2026
Revised: 20 March 2026
Accepted: 26 March 2026
Published: 12 April 2026

Abstract

Upper troposphere (UT) humidity records are crucial for climate studies. To maximize temporal representativeness and enhance the lidar signal, pseudo-monthly averaging—limited to nighttime measurement—is applied, yielding water vapor mixing ratio (WVMR) profiles up to 16 km. This study evaluates 11 years (2013–2023) of WVMR profiles from a UV Raman lidar (Li1200) at Réunion Island, comparing them with MLS-Aura satellite retrievals, ERA5 reanalysis data, and GRUAN-processed M10 radiosondes. The results reveal a systematic dry shift in MLS of up to 30% above 12 km, particularly during the wet season. The lidar exhibits a slight downward shift in WVMR, approximately 5% lower than ERA5 throughout the UT, with the largest deviations occurring above 14 km and greater variability during the wet season. Calibration-related challenges during the dry season result in lidar WVMR profiles that are up to 10% drier than ERA5. Additionally, comparisons with GRUAN-processed radiosondes show a substantial dry shift relative to the lidar, exceeding 30% above 12 km. We investigate the effect of GNSS-based lidar calibration by applying an alternative calibration method, which produces higher WVMR values. This reveals a dry shift in ERA5 relative to the lidar, increasing with altitude in the UT up to 25%. These measurements contribute to the global effort to monitor and validate tropical and subtropical upper tropospheric humidity.

Keywords: upper tropospheric humidity; pseudo-monthly; Raman lidar; MLS-Aura; ERA5 reanalysis; GRUAN-analyzed radiosondes; water vapor mixing ratio

1. Introduction

Tropical and subtropical upper tropospheric water vapor plays a central role in climate feedback and radiative energy balance (IPCC report of 2023). Even small variations in humidity at these altitudes can disproportionately impact outgoing longwave radiation, making upper tropospheric moisture one of the most sensitive amplifiers of climate change.

The Global Climate Observing System (GCOS) identifies upper-air water vapor as an Essential Climate Variable, prioritizing the reduction in observational gaps through improved data quality and long-term measurement capabilities (WMO report of 2022). Improved observations also help constrain stratosphere–troposphere exchange processes, refine representations of moist convection in models, and reduce uncertainties in climate sensitivity projections [1–5].

A variety of techniques exist for measuring atmospheric water vapor, including in situ, ground-based, airborne, and satellite remote sensing [5–7]. Among these, spaceborne observations provide global coverage across multiple atmospheric layers. However, few satellite instruments can reliably retrieve detailed vertical distributions of water vapor in the upper troposphere (UT) with sufficient accuracy and vertical resolution [8–10].

The Microwave Limb Sounder (MLS) [11], aboard NASA's Aura satellite, is a reliable instrument for retrieving water vapor information in the UT and lower stratosphere (LS). Despite its broad coverage and long-term continuity, MLS retrievals are affected by uncertainties under humid and dynamically variable upper tropospheric conditions. Comparisons with independent datasets [9,10,12,13] provide valuable insights into satellite performance. This study contributes to ongoing evaluation efforts by examining 11 years (2013–2023) of MLS data over a subtropical site.

In situ measurements from radiosondes provide valuable reference data, although instruments equipped with capacitive sensors are generally unreliable in the UT. Frost point hygrometers, such as the Cryogenic Frost point Hygrometer (CFH), offer superior accuracy,

with uncertainties of 2–4% in the tropical lower troposphere, 5–9% near the tropopause, and approximately 10% at 28 km [14,15]. CFHs have been used to assess tropical humidity variability and trends [16] and to validate satellite-derived upper-tropospheric water vapor [14]. However, their high cost and sensitivity to spatiotemporal mismatches limit their routine deployment. Operational radiosondes, if robust against harsh conditions—as demonstrated by GCOS Reference Upper-Air Network (GRUAN)-certified instruments [17]—represent a promising alternative. However, such data have only been available at Réunion Island since November 2019 and have not been previously validated, to our knowledge. In this study, we examine 4 years (2019–2023) of GRUAN-analyzed Meteomodem M10 radiosonde humidity data in the UT.

Representing humidity in the UT remains a major challenge for atmospheric models [18]. ERA5 [19], the fifth-generation reanalysis from the European Centre for Medium-Range Weather Forecasts (ECMWF), provides long-term global information on upper tropospheric moisture. However, its uncertainties in this region can be questioned when compared to assimilated radiosonde and satellite data. The hourly ERA5 dataset, available on 37 pressure levels [20], is also examined in the UT in this study, as it is available at the subtropical site for the same period.

Airborne in situ measurements further complement remote sensing. The In-service Aircraft for a Global Observing System (IAGOS; www.iagos.org, last accessed on 25 March 2026) database provides H_2O observations from passenger aircraft, capturing strong vertical and temporal variability in the UT/LS over the extratropical Northern Hemisphere. However, these observations mainly cover North America, the North Atlantic, and Europe (40–60° N) and are not available over the Reunion Island region [21].

The Network for the Detection of Atmospheric Composition Change (NDACC; https://ndacc.larc.nasa.gov/, last accessed on 25 March 2026) was designed to monitor the middle atmosphere [22]. However, the UT/LS section was identified as poorly covered, while radiosondes and GNSS-RO errors increase in this region, and space observations have limitations in terms of vertical resolution and coverage down to the stratosphere. Ground-based Raman lidars offer a highly reliable reference for upper tropospheric water vapor, providing high vertical resolution and continuous WVMR profiles suitable for trend studies. For example, lidars at Zugspitze (Germany) [23], Table Mountain Facility (United States) [24,25], Tor Vergata (Italy) [26], and the Observatory of Haute-Province (France) [27] can reach UT altitudes, up to the lower tropopause in mid-latitude regions. Most of these systems contribute to NDACC [22], which is characterized as a high-quality global atmospheric-sounding network. However, the range is not fully satisfactory. Based on the experiences at Observatory of Haute-Provence and with a preliminary system at La Reunion on both of the existing Rayleigh lidar systems, a specific system was designed for water vapor monitoring. This system features a larger telescope (1.2 m diameter) and two powerful lasers, is located at high altitude at Maïdo Observatory (2160 m a.s.l), and has been operating since 2012 [28]. It monitors water vapor from the surface to the LS and simultaneously measures stratospheric and mesospheric temperatures. Campaigns conducted since 2013 [26,29,30] have demonstrated the lidar's ability to detect WVMR as low as a few parts per million by volume (ppmv) in the UT/LS and to reach subtropical UT/LS altitudes through extended Raman integration [30]. To further increase the altitude range, simulations by Verémes and colleagues [30] suggest that averaging larger lidar datasets over several consecutive measurement periods can extend the altitude range. Following this approach, and based on monthly averaging of nighttime lidar measurements (hereafter named pseudo-monthly), we evaluate upper tropospheric WVMR profiles retrieved by the Li1200 over 11 years (2013–2023). This temporal screening enables comparisons with MLS retrievals, ERA5 outputs, and GRUAN-analyzed radiosondes over the UT above Reunion

Island. The objectives of this study are to assess the reliability of these multi-source water vapor datasets in the UT and to evaluate the Li1200 dataset. Future work will test the potential applicability of these datasets to climate and atmospheric studies. Section 2 presents the Materials and Methods, including the Li1200 lidar and the additional datasets used in this study. Section 3 describes the main comparison results, and Section 4 presents the discussions, including an alternative lidar calibration, before the conclusions.

2. Materials and Methods

2.1. The Li1200 Lidar

The Raman lidar has been operating at the Maïdo Observatory on Réunion Island (21°S, 55.4°E) since 2012 [28]. In 2013, the system was upgraded to operate at a 355 nm emission wavelength, which provides more efficient Raman detection compared to the previous 532 nm configuration [26]. The system employs two Quanta Ray Nd:Yag lasers provided by MKS Spectra-Physics co. (Santa Clara, CA, USA) operating at 30 Hz to generate laser pulses. The dual-laser configuration significantly increases the emitted power, with both lasers synchronized using a pulse generator module that ensures timing uncertainty below 20 ns. Each laser emits 375 mJ per pulse with a duration of 9 ns, and the beams are combined using a polarization cube.

The transmitter and receiver share a coaxial geometry, which minimizes parallax effects, enables measurements close to the surface, and facilitates optical alignment. Backscattered photons are collected by a Newtonian telescope with a 1200 mm primary mirror, from which the system derives its name, "Li1200".

Since Raman scattering from water vapor is significantly weaker than elastic backscatter, minimizing fluorescence sources in the detection chain is crucial. Optical fibers, known to induce fluorescence that can introduce systematic biases in Raman measurements [31], are not used in this system due to coupling losses. Instead, an optical box is placed directly after the telescope to spectrally separate the Raman and Rayleigh returns. A diaphragm field stop at the entrance of this separation unit allows for an adjustable field of view (FOV) ranging from 3 to 0.5 mrad. During routine operations, an FOV of 2 mm (0.5 mrad) is selected to reduce background light and prevent photomultiplier saturation from strong low-altitude elastic scattering.

Spectral selection is achieved using a series of dichroic beam splitters and interference filters, which separate the backscattered signal into its Raman and elastic components. Signal detection is performed using Hamamatsu miniature photomultiplier tubes (PMTs), and data acquisition is carried out using Licel transient recorders (Licel GmbH, Berlin, Germany) operating in photon-counting mode [30] (V2.43 of Licel software).

In addition to routine observations, the Li1200 system has participated in five intensive measurement campaigns. These campaigns, with increased sampling frequency, enabled extensive testing of various optical configurations, leading to the selection of the current operational setup, as detailed in [26].

The overlap function is nearly identical for both Raman and elastic channels, allowing water vapor profiles to be retrieved down to near the surface. Water vapor mixing ratio profiles are derived from the ratio of Raman backscatter signals detected at 408 nm (water vapor; [31]) and 387 nm (nitrogen; [32]). These signals, recorded as photon counts per altitude bin per laser shot, are corrected for background noise, adjusted for the differential atmospheric transmission T(z), and scaled by a calibration coefficient C.

The full processing chain, including uncertainty characterization and determination of the effective vertical resolution, is described in [30,32]. This includes the uncertainty associated with calibration using collocated GNSS-integrated water vapor (IWV) measurements. These measurements are retrieved via the GNSS TRIMBLE-NETR9 receiver (Trimble

Inc., Sunnyvale, CA, USA; MAIG, http://rgp.ign.fr/STATIONS/#MAIG, last accessed on 30 March 2026), which has been operational at the Maido observatory since 2013. IWV is derived from the Zenithal Wet Delay (ZWD), which represents the atmospheric propagation delay of GNSS signals primarily due to water vapor abundance. ZWD is converted into IWV using surface temperature and empirical formulas [33], with surface pressure and temperature data sourced from a meteorological station collocated with the lidar. The uncertainty in GNSS IWV arises from the uncertainty in the total delay (ZTD), provided by Gipsy-Oasis, and the uncertainty of the pressure and temperature sensors of the meteorological station, as determined by the sensor's datasheet. The accuracy of GNSS IWV is approximately 1 mm, corresponding to relative uncertainties of 6–18% depending on season and total atmospheric water vapor content [34].

Under routine operating conditions, the lidar system described in [26] provides water vapor profiles up to approximately 15 km. The primary limitations affecting retrievals near the tropopause and the detection of fine-scale UTLS structures—particularly in the presence of horizontal advection—are statistical uncertainties inherent in photon-counting detection. These uncertainties scale with the square root of the measured signal and depend on both vertical filtering and temporal averaging. Background noise also imposes significant constraints, which is why water vapor measurements from this Raman lidar are limited to nighttime periods.

The native vertical resolution of the lidar measurements is 15 m. To reduce high-frequency noise, the profiles are smoothed using a low-pass filter based on a Blackman window, which provides sharp spectral filtering. Since noise increases with altitude, the number of smoothing points is increased with height to compensate for the reduced signal-to-noise ratio (SNR). The NDACC community has adopted two standard methods for defining the effective vertical resolution of lidar profiles: (i) the full width at half maximum (FWHM) of the finite impulse response [35], and (ii) the cut-off frequency of the digital filter, the latter being applied to the Li1200 data. Using the number of points employed in the Blackman filter at each altitude level, the corresponding vertical resolutions range from approximately 100 to 200 m in the lower troposphere, to about 500 m in the mid-troposphere, and around 600 m in the upper troposphere.

Longer temporal averaging of the Raman signals increases the lidar signal-to-noise ratio, thereby extending the usable altitude range of the WVMR profiles. Vérèmes et al., 2019 [30] demonstrated that a 10-min integration typically provides reliable water vapor retrievals up to approximately 14 km, while 40-min integrations allow profiles to reach even higher altitudes. Following this principle, we apply a pseudo-monthly integration strategy, in which Raman signals are accumulated over several successive nighttime periods within each month, yielding a total integration time of at least 1920 min. Figure 1 shows an example of a single-night WVMR profile reaching about 14 km, alongside the pseudo-monthly WVMR profile for the same month, which reaches over 16 km. This newly constructed pseudo-monthly dataset provides a more suitable basis for comparisons with satellite measurements and climatological studies. To further improve the robustness of the comparisons, all lidar data points with relative uncertainty exceeding 30% are excluded. Using this approach, we produced 100 pseudo-monthly WVMR profiles for the period 2013–2023, each with a vertical extent determined by its total accumulated signal.

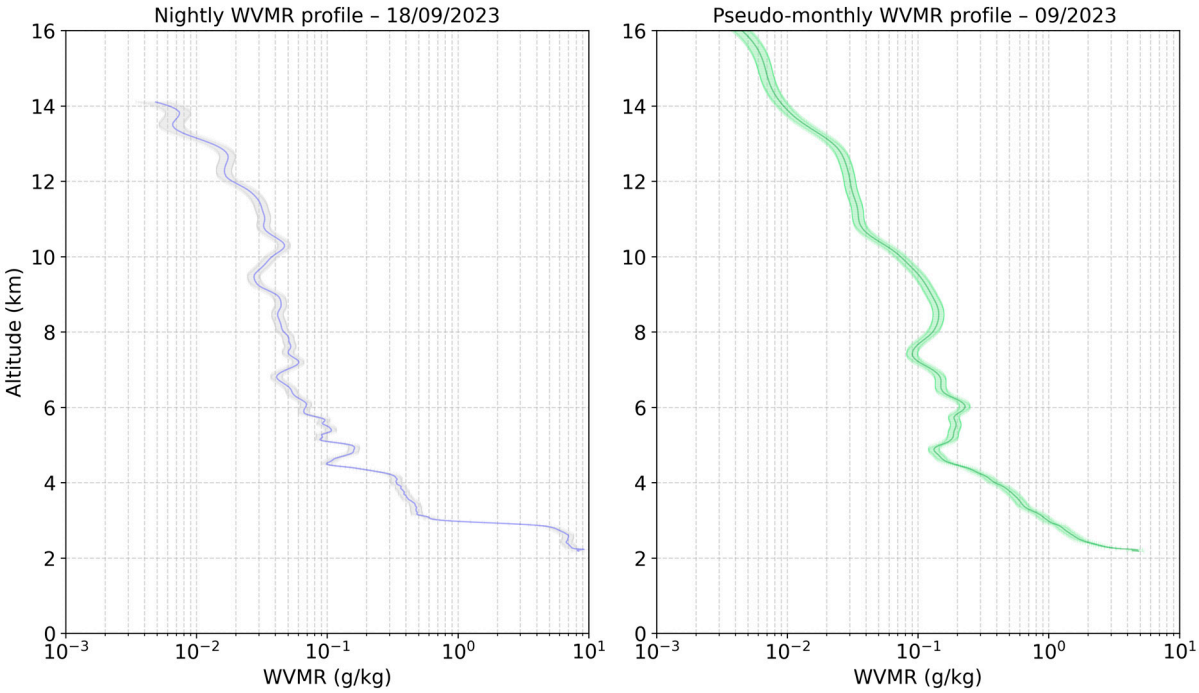

Figure 1. Lidar WVMR profile (in g/kg). (**Left panel**): single-night profile for 18 September 2023. (**Right panel**): pseudo-monthly profile for September 2023. Shaded areas indicate the lidar profile uncertainty.

2.2. Microwave Limb Sounder (MLS)

The Earth Observing System Microwave Limb Sounder (EOS MLS; hereafter MLS), operational since July 2004 aboard the Aura spacecraft, measures microwave radiances from the limb. These radiances are inverted to obtain profiles of temperature, geopotential height, cloud ice, and several trace gases, including the water vapor mixing ratio from the UT (316 hPa) to the stratosphere [11]. MLS retrievals are horizontally spaced by 165 km (1.5°) along the orbit track, with roughly 15 orbits per day [36]. The maximum global retrieval rate is 3494 profiles per day, providing near-global spatial coverage from −82° to +82° latitude. The recommended useful vertical range extends from 316 hPa to 0.00215 hPa, with a vertical resolution of approximately 1.5 km at 316 hPa and 3.5 km at 4.64 hPa, degrading to 15 km above 0.1 hPa.

The present study uses Version 5 in the Level 2 Geophysical Product (L2GP) files (MLS-Aura_L2GP-H2O_v05-00-c01) of water vapor retrievals, which are publicly available from the Goddard Space Flight Center DAAC at https://mls.jpl.nasa.gov/ (last accessed on 25 March 2026). Further information about this version is available in the MLS v5.0 Data Quality Document (https://mls.jpl.nasa.gov/data/v5-0_data_quality_document.pdf; last accessed on 25 March 2026). We adhere to the recommended vertical range for data use, spanning 316–0.001 hPa.

Biases in Aura MLS are well characterized globally, with multiple validation studies conducted for water vapor [9,13,37–41].

No previous studies have validated the multi-year record of MLS over Reunion island. In this study, we focus on evaluating WVMR profiles over the 10–16 km altitude range, which corresponds to a vertical resolution of approximately 1.1 km and a maximum horizontal shift of ~4° from the Maïdo Observatory (the lidar location). To enable comparison with the Li1200 observations, only nocturnal MLS overpasses collocated with the lidar site—typically around 21:00–22:00 local time—are considered. From these, 76 pseudo-monthly MLS WVMR profiles were generated for comparison with coincident lidar measurements between 2013

and 2023. Two examples—a single-night WVMR profile and the pseudo-monthly WVMR for the same month over the subtropical upper troposphere site—are presented in Figure 2, showing data from both the lidar and MLS.

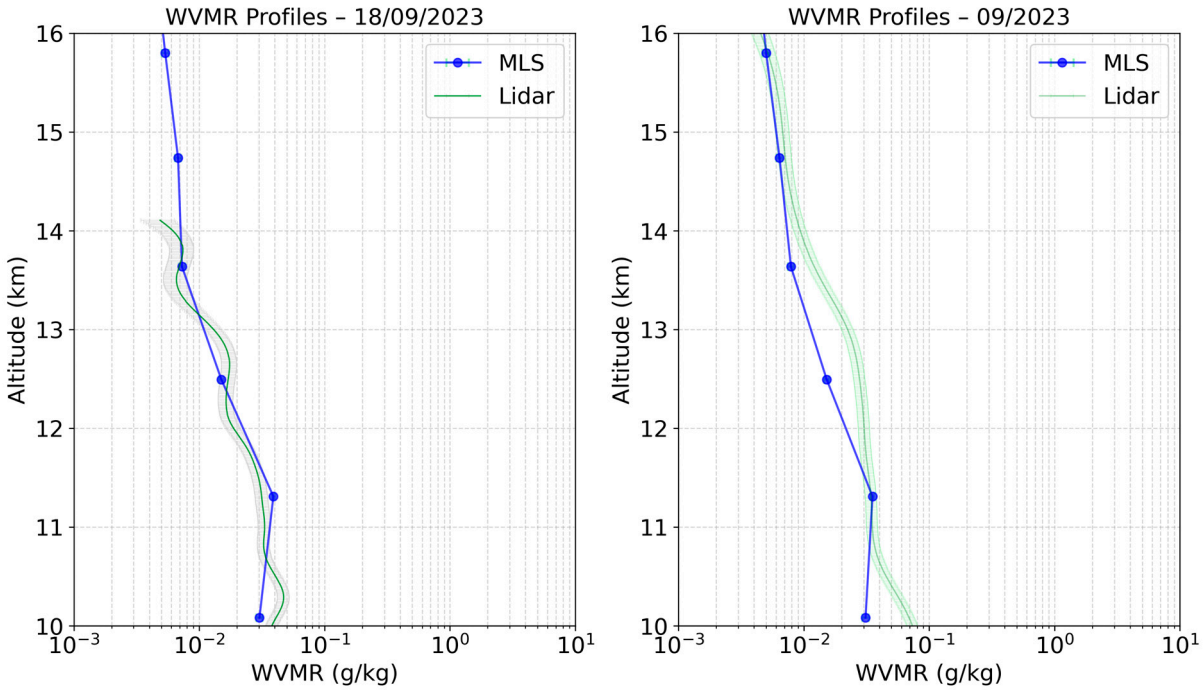

Figure 2. WVMR profiles (in g/kg) from lidar and MLS-Aura Satellite over 10–16 km. (**Left panel**): single-night profile for 18 September 2023. (**Right panel**): pseudo-monthly profile for September 2023. Shaded areas indicate the lidar profile uncertainty. The MLS profile uncertainty is <5% mostly.

2.3. ERA5 Re-Analysis

ERA5 represents the fifth generation of the atmospheric meteorological reanalysis produced by the European Centre for Medium-Range Weather Forecasts (ECMWF), and it has been operational since 2016 [19]. ERA5 benefits from a decade of advancements in model physics, core dynamics and data assimilation, which guide and refine the outputs of interactive models. The ERA5 dataset [20] features a significantly enhanced horizontal resolution of 31 km (0.25°), compared to the 80 km resolution of its predecessor, ERA-Interim. It provides hourly output across 37 pressure levels and offers a detailed, publicly available record of the global atmosphere from 1979 onward (with less frequent data between 1950 and 1979). Over time, the uncertainty in tropospheric humidity samples, primarily due to random errors, has decreased. The relative spread is lowest near the surface, at around 5%, but it has been approximately 15% for specific humidity at 300 hPa since 2015 [19].

WVMR is calculated from the specific humidity variable at the ERA5 grid point closest to the lidar location, the Maido Observatory. To align with the lidar observations, data are selected with a maximum horizontal (spatial) drift of 0.1° and the best temporal coincidence with nighttime lidar measurements. Using this approach, 91 pseudo-monthly ERA5 WVMR profiles were retrieved for the period from 2013 to 2023, enabling direct comparison with the Li1200 profiles. Figure 3 presents two examples of WVMR profiles: one from a single lidar-like night and another from a pseudo-monthly lidar-like period, both from ERA5 and the lidar.

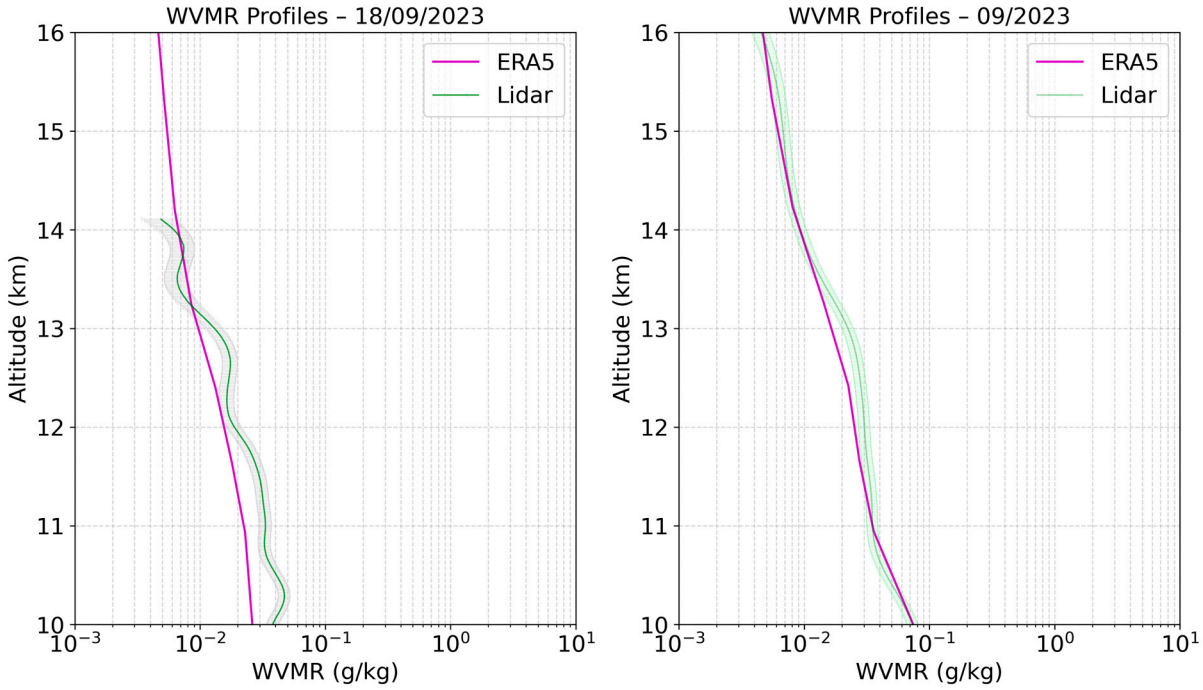

Figure 3. WVMR profiles (in g/kg) from ERA5 and lidar over 10–16 km. (**Left panel**): lidar-like night profile for 18 September 2023. (**Right panel**): pseudo-monthly profile for September 2023, Shaded areas indicate the lidar WVMR error.

2.4. GRUAN-Processed Meteomodem M10 Radiosondes

Balloon-borne radiosondes provide local humidity profiles above the launch site, although spatial collocation with fixed-point measurements can be influenced by wind speed and direction at altitudes where the balloons drifts. To approximate the location of the lidar, we used data from the Gillot meteorological station (also referred to as Chaudron in the data files, WMO code 61980) in Saint-Denis (20.9°S, 55.5°E, 46 m a.s.l). At this station, Meteomodem Co. (www.meteomodem.com, Ury 77760, France; URL last accessed on 25 March 2026) M10 radiosondes are regularly launched at midnight and midday. To ensure reference-quality and thus better climate-quality measurements, this station's radiosonde dataset benefits from regular processing, coordinated by GRUAN [42], which provides well-calibrated water vapor measurements. For M10 radiosondes, several corrections are applied to meet GRUAN standards [42]. These corrections, detailed in Dupont et al. (2020) [43], include (1) calibration adjustments; (2) corrections for slow sensor response, particularly at extreme humidity levels; (3) compensation for relative humidity sensor dependence on temperature gradients; and (4) time-lag corrections at cold temperatures which affect measurements in regions with strong relative humidity gradients.

The WVMR profiles used in the present study are derived from the corrected relative humidity (with all GRUAN corrections applied) [43], along with air temperature and pressure levels from the M10 radiosondes launched at midnight. Between November 2019 and December 2023, 41 GRUAN-processed M10 WVMR profiles were retrieved and compared with coincident lidar measurements at the pseudo-monthly scale. Figure 4 illustrates two examples: a single midnight launch WVMR profile and the pseudo-monthly profile from both the lidar and GRUAN-processed M10 radiosondes in the UT.

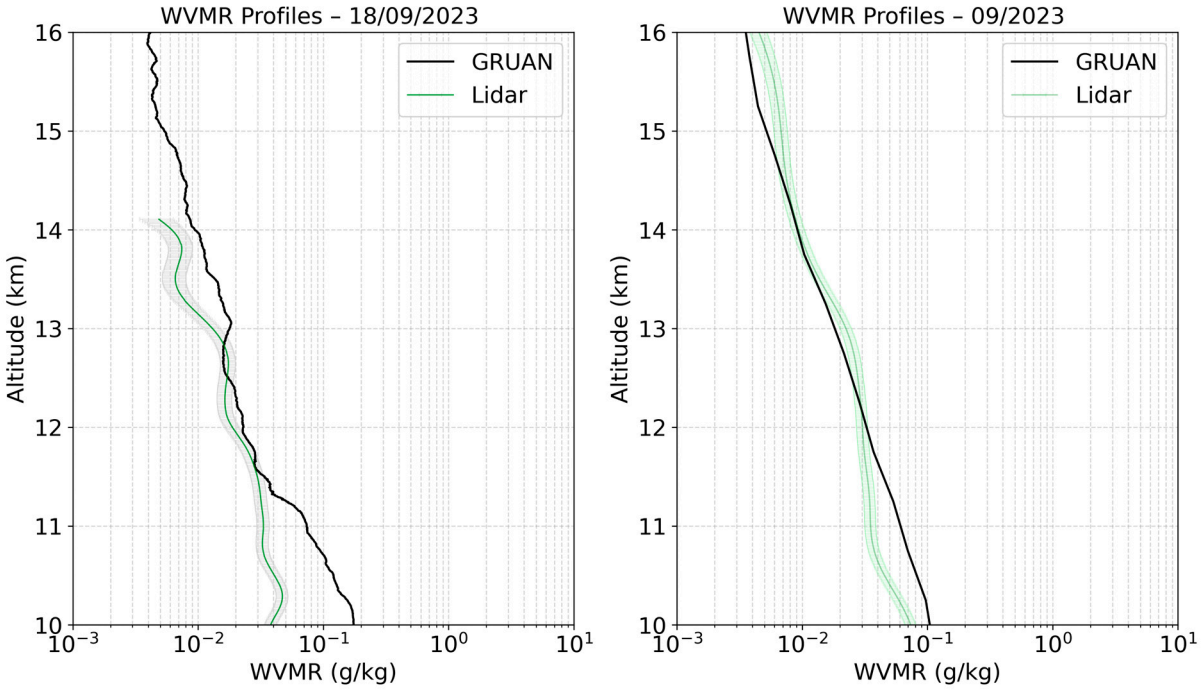

Figure 4. WVMR profiles (in g/kg) from both lidar and GRUAN-processed M10 radiosonde over 10–16 km. (**Left panel**): single night profile for 18 September 2023, (**Right panel**): pseudo-monthly profile for September 2023. Shaded areas indicate lidar WVMR error.

A preliminary examination of WVMR profiles in the UT from all three compared datasets (Figures 2–4) reveals close agreement, particularly at the monthly scale. To gain deeper insights, a statistical comparison was subsequently conducted, with the main results presented in the following section.

3. Results

A central challenge of this study is the limited number of true nocturnal satellite overpasses that are suitable for direct comparison with lidar-derived WVMR profiles. The pseudo-monthly WVMR dataset, generated from lidar, MLS, ERA5, and GRUAN nocturnal observations, helps overcome this limitation. This temporal aggregation maximizes the number of usable MLS overpasses and enhances the robustness of comparisons in the upper troposphere. It also leverages the lidar's capability to probe water vapor at higher altitudes through long-duration Raman signal accumulation. All comparisons are conducted relative to the Raman lidar, with relative differences used to characterize the uncertainties of each dataset. However, gaps inevitably occur in the pseudo-monthly time series, primarily during periods without valid observations. These gaps can be attributed to instrument downtime, COVID-19-related disruptions, or profiles failing to meet the quality criteria (with relative errors exceeding 30%).

3.1. LIDAR vs. MLS-Aura

Relative differences between the Li1200 lidar and MLS WVMR profiles were examined over the 10–16 km altitude range, where both instruments provide robust measurements. For each month, all MLS observations that coincided with nighttime lidar measurements were averaged to create a representative pseudo-monthly profile. Over the period from 2013 to 2023, this process resulted in 76 pairs of lidar–MLS pseudo-monthly profiles, all of which were interpolated to the vertical resolution of MLS.

The median relative difference in WVMR between the Li1200 lidar and MLS over the 11-year period is illustrated in Figure 5 (black dashed line), along with the 95% confi-

dence interval of the variability (blue shading). The confidence bounds were calculated as ±2 times the pseudo–standard error, normalized by the square root of the number of contributing profile pairs in each altitude bin. The smallest differences occur between 11 and 12 km, while the lidar reports values up to 30% higher at altitudes above this layer. The spread increases above 14 km, which is consistent with reduced lidar sensitivity and the coarser vertical resolution of MLS at higher altitudes. This dry shift in MLS relative to the lidar in the UT aligns with previous investigations [9,38], and similar magnitudes have been reported over Reunion Island in earlier, shorter–term lidar–satellite comparisons (e.g., [26]).

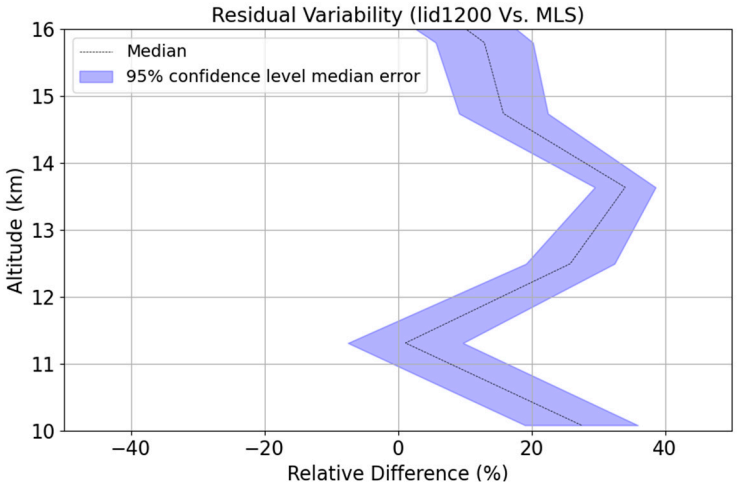

Figure 5. Median relative shift (%) of Li1200 WVMR with respect to MLS over 76 compared pseudo-monthly profile pairs from 2013 to 2023. Shaded areas indicate the 95% confidence interval of the relative error.

Next, we investigate the temporal evolution of the relative differences (Li1200—MLS) over the entire period at two representative altitude levels (Figure 6): 11.3 km and 13.7 km. These altitudes were chosen because the median shift exhibits different magnitudes at these levels (as shown in Figure 5). Significant interannual variability is observed in the data. At 13 km (blue bars), the relative differences indicate a dominant dry shift in MLS (Li1200 > MLS). At 11 km (red bars), differences are also substantial but show a more stable trend around 0%, although occasional extreme peaks are still present. The dominant dry shift in MLS is particularly evident at both altitudes during 2018 and 2019.

Some gaps in the time series correspond to periods with insufficient MLS and lidar observations to generate a representative pseudo-monthly pair. For example, these gaps can occur when there is only a single night of observation during a given month.

To further explore seasonal influences, the analysis was divided into two main subtropical seasons: the dry season (May–September) and the wet season (October–April). The relative differences exhibit a distinct structure during the wet season (Figure 7a), with a clear dry shift in MLS reaching up to 40% between 12 and 14 km. This may reflect improved lidar sensitivity under moister conditions, which reduces calibration-related limitations and enhances the lidar's performance in the UT. The dry shift in MLS is also observed during the dry season (Figure 7c) across most upper tropospheric altitudes, except near 11 km, where the relative differences show a slightly more stable trend around 0%. The smaller magnitude of the MLS dry shift relative to the lidar during the dry season could be attributed to mutual complications in water vapor measurements under drier conditions. Figure 7b,d show the median WVMR profiles during the wet and dry seasons, respectively. All analyses are based on data from the 2013–2023 period (11 years).

Figure 6. Temporal evolution of relative differences (%) between Li1200 and MLS (Li1200—MLS) at 13 km (blue) and 11 km (red) from 2013 to 2023. Positive values indicate that Li1200 reports higher WVMR than MLS. Gaps correspond to months with insufficient coincident observations.

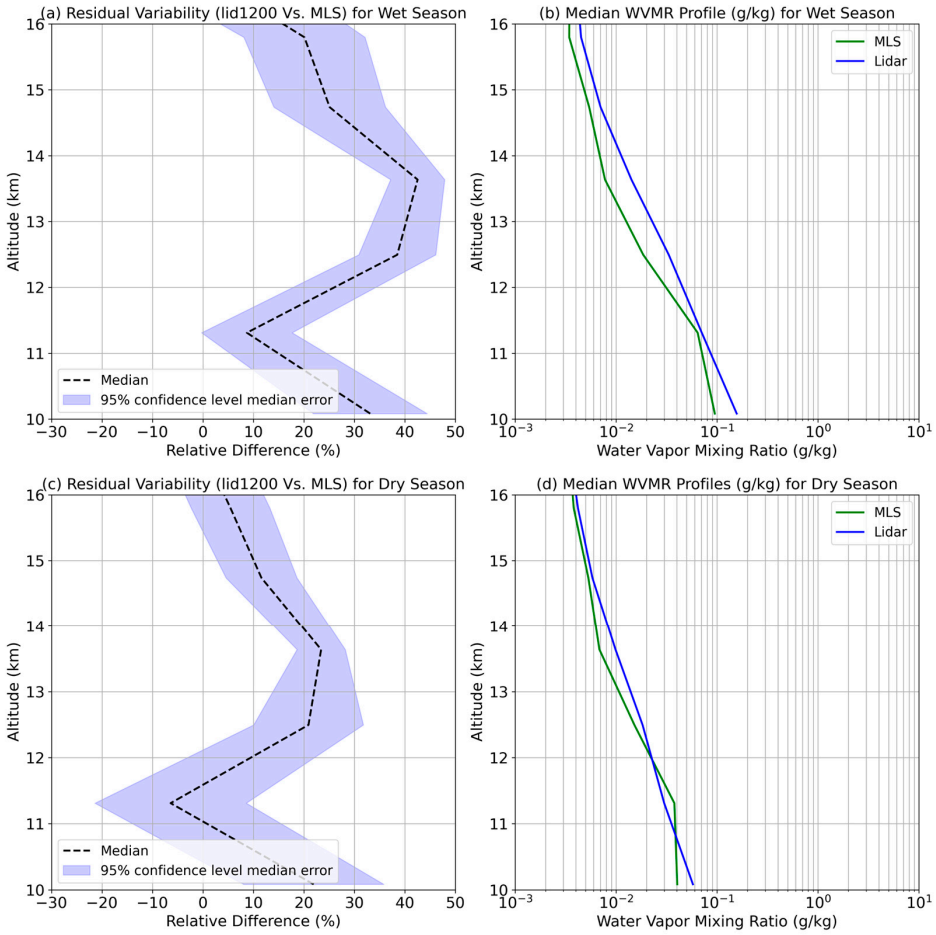

Figure 7. Seasonal comparison of Li1200 WVMR relative to MLS over the 2013–2023 period. (**a**) Median relative lidar to MLS shift (%) during wet season months (October–April); (**b**) Median WVMR profile (g/kg) during the wet season; (**c**) Median relative shift (%) during dry season months (May–September); (**d**) Median WVMR profile (g/kg) during the dry season. Shaded areas indicate the 95% confidence interval of the median relative error.

3.2. LIDAR vs. ERA5

The relative differences between the Li1200-derived WVMR and ERA5 reanalysis were also evaluated on a pseudo-monthly basis over the subtropical site. For each month, ERA5 hourly profiles that coincided with nighttime lidar measurements were averaged to construct a representative pseudo-nightly profile, which was then aggregated into a pseudo-monthly profile. The comparison focuses on the 10–16 km altitude range. Over the 2013–2023 period, a total of 91 pseudo-monthly WVMR profiles were generated. The overall shift of lidar relative to ERA5 is summarized by the median of these 91 relative-difference profiles, with ERA5 showing a small wet shift reaching approximately 5% (Figure 8). We further examined the temporal evolution of the relative differences (Li1200—ERA5) at two representative altitude levels (Figure 9): 11 km and 14 km, where the median shift differs slightly (Figure 8). Positive values indicate a dry shift in ERA5 (Li1200 > ERA5), while negative values indicate a wet shift (Li1200 < ERA5). At 14 km (blue bars), the relative differences indicate a dominant dry shift in ERA5 after 2018. However, enhanced variability prior to 2018 reduces the overall median shift to approximately 0% (Figure 8). At 11 km, Li1200 values were mostly drier than those of ERA5 until 2021, after which the shift reverses slightly, resulting in a small dry shift in Li1200 of up to 5% relative to ERA5.

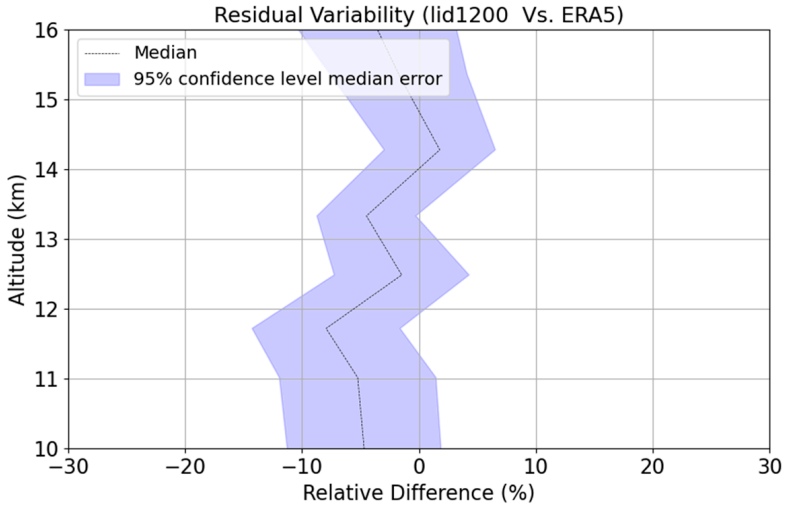

Figure 8. Median relative bias (%) of Li1200 WVMR with respect to ERA5 over 91 pseudo-monthly profiles from 2013 to 2023. Shaded areas indicate the 95% confidence interval of the relative error.

The analysis was further divided into the two dominant subtropical seasons, revealing distinct patterns in the relative differences between Li1200 and ERA5 datasets. During the wet season (Figure 10a), a small dry shift in ERA5, reaching approximately 5%, persists at upper altitudes above 14 km. This shift may be attributed to model assumptions in ERA5 within the UT. Below 14 km, the variability of the shift is generally larger, with Li1200 values tending to be drier than those of ERA5 by up to 10%. This variability may reflect calibration-related uncertainties in the lidar measurements. The effect is even more pronounced during the dry season (Figure 10c) throughout most of the profile. Figure 10b,d show the seasonal median WVMR profiles for the wet and dry seasons, respectively. All analyses are based on data from the 2013–2023 period (11 years).

Figure 9. Temporal evolution of relative differences (%) between Li1200 and ERA5 (Li1200—ERA5) at 14 km (blue) and 11 km (red) from 2013 to 2023. Positive values indicate that Li1200 reports higher WVMR than ERA5. Gaps correspond to months with insufficient lidar observations.

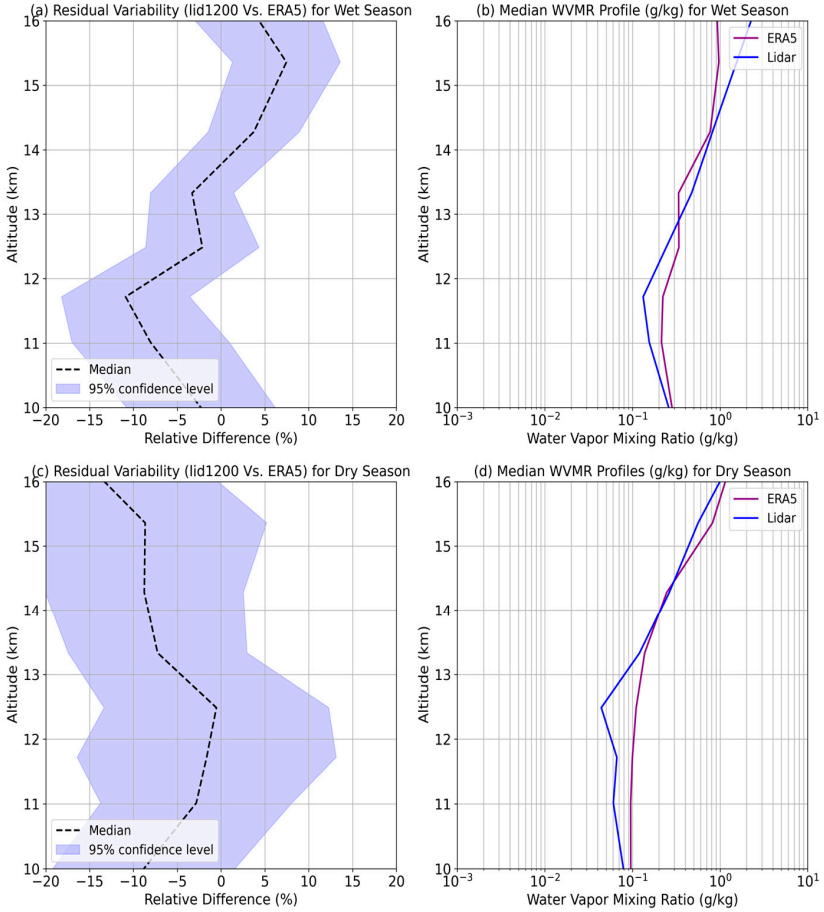

Figure 10. Seasonal comparison of Li1200 WVMR relative to ERA5 over the 2013–2023 period. (**a**) Median relative shift (%) during wet season months (October–April); (**b**) Median WVMR profile (g/kg) during the wet season; (**c**) Median relative shift (%) during dry season months (May–September); (**d**) Median WVMR profile (g/kg) during the dry season. Shaded areas indicate the 95% confidence interval of the median relative error.

3.3. Li1200 vs. GRUAN-Processed M10 Radiosondes

The relative differences between Li1200-derived WVMR and GRUAN-processed M10 radiosondes were also evaluated on a pseudo-monthly basis. For each month, all GRUAN midnight soundings that coincided with nighttime lidar measurements were averaged. The comparison focuses on the 10–16 km altitude range over the 2019–2023 period, during which 41 pseudo-monthly profiles were retrieved. The shift in lidar measurements relative to GRUAN is defined as the median of all relative-difference profiles. Below 12 km, the Li1200 exhibits a small dry shift relative to the radiosondes, at approximately 10% (Lidar < GRUAN). Above 12 km, this shift reverses, with the lidar showing approximately 20% higher values at 14 km and up to 40% higher values at 16 km (Lidar > GRUAN), as shown in Figure 11. We further investigated the temporal evolution of these relative differences at two representative altitudes: 11 km and 14 km.

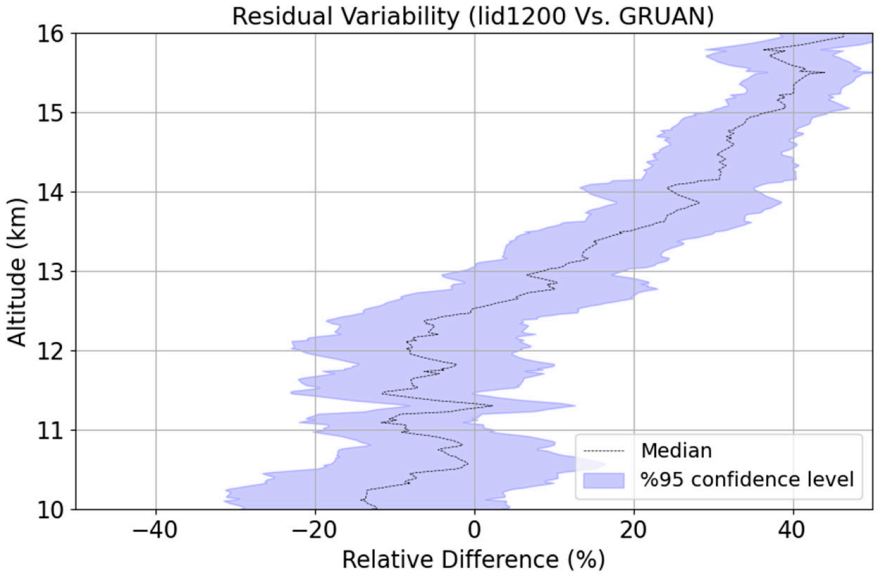

Figure 11. Median relative shift (%) of Li1200 WVMR with respect to GRUAN-processed M10 radiosondes over 41 pseudo-monthly profiles from 2019 to 2023. Shaded areas indicate the 95% confidence interval of the relative error.

Above 12 km, GRUAN radiosondes exhibit a pronounced dry shift relative to the lidar in both seasons (Figure 12, blue bars). Seasonal stratification reveals clear differences between the wet and dry periods (Figure 13). Below 12 km, this shift reverses, with Li1200 values being approximately 10% lower than those of GRUAN M10 during the wet season (Figure 13a). However, enhanced variability (Figure 12, red bars) reduces the overall median shift to approximately 0% during drier conditions (Figure 13c). Enhanced column humidity may increase the strength of Raman backscatter, reducing calibration-related limitations and thereby improving upper-tropospheric WVMR values. This explains the larger shift relative to radiosondes above 12 km. Meanwhile, spatial mismatches between the radiosonde ascent and the lidar location—particularly when trajectories drift toward the southwest Indian Ocean—can amplify discrepancies during wet conditions, explaining the wetter-than-lidar shifts observed below 12 km.

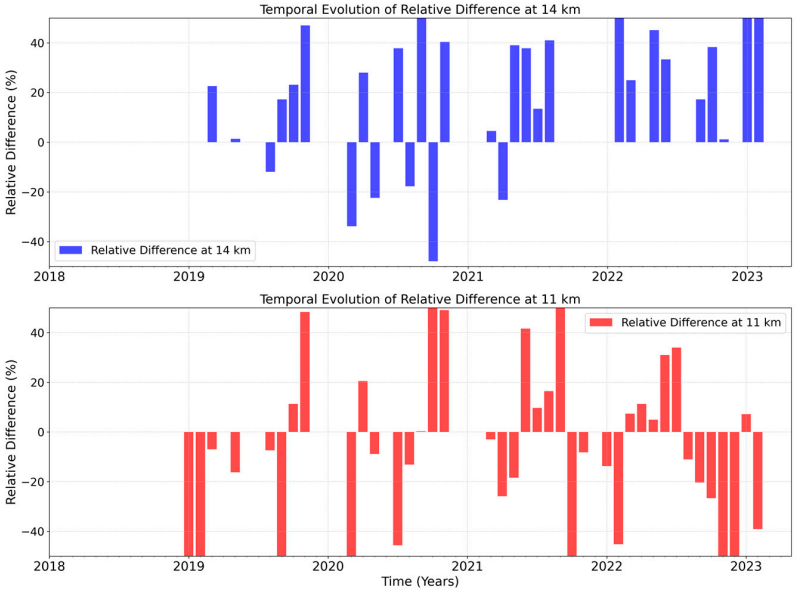

Figure 12. Temporal evolution of relative differences (%) between Li1200 and GRUAN-processed M10 (Li1200—GRUAN) at 14 km (blue) and 11 km (red) from 2019 to 2023. Positive values indicate that Li1200 reports higher WVMR. Gaps correspond to months with insufficient lidar observations.

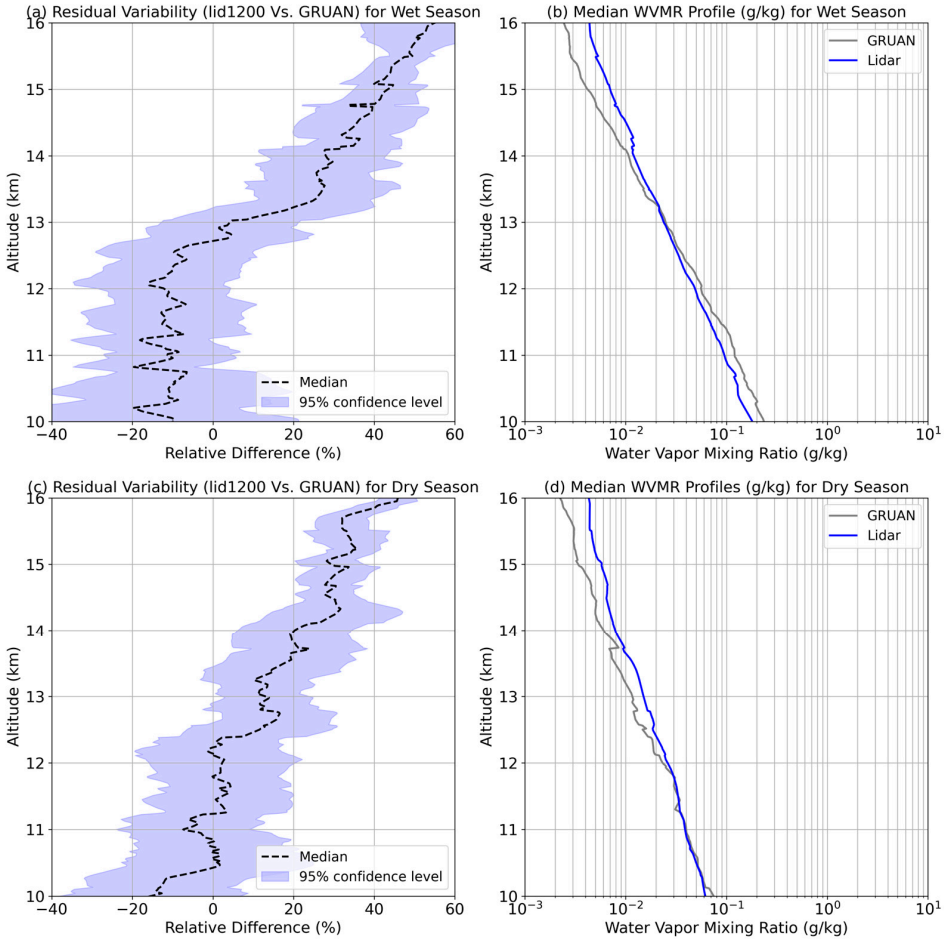

Figure 13. Seasonal comparison of Li1200 WVMR relative to GRUAN-processed M10 radiosondes. (**a**) Median relative shift of Li1200 relative to radiosondes (%) during wet season months (October–April). (**b**) Median WVMR profile (g/kg) during the wet season. (**c**) Median relative Li1200 shift (%) during the dry season months (May–September). (**d**) Median WVMR profile (g/kg) during the dry season. Shaded areas indicate the 95% confidence interval of the median relative error.

4. Discussion

Our results indicate that both satellite MLS and GRUAN-processed M10 radiosondes exhibit an upper-tropospheric dry shift relative to Li1200 WVMR profiles at pseudo-monthly timescales. However, Li1200 measurements remain slightly drier than those from ERA5. A central question arises: How accurate are Raman lidar observations of upper tropospheric water vapor using UV (355 nm emission, as with Li1200) over the subtropics?

One possible source of uncertainty is aerosol-induced fluorescence, as previously discussed by Chouza et al. (2022) [44] at the same site using the same lidar system. This effect can lead to wetter lidar values and may partially explain the dry shifts observed in MLS and GRUAN-processed M10 measurements. Even if Raman lidars were influenced by aerosols, they would still tend to be drier than ERA5.

Another consideration is the spatial representativity of GRUAN radiosondes. The launch site at Saint-Denis airport may be sufficiently distant, and radiosonde drift could carry measurements toward the ocean, resulting in vertical profiles that are not fully collocated with the lidar. To investigate this, we analyzed radiosonde trajectories between altitudes of 10 and 16 km (Figure 14). The trajectories predominantly drift up to 100 km toward the east/southeast from the launch site. A comparative analysis was performed, separating GRUAN M10 soundings into "near" and "far" drift classes relative to the lidar location. These classes were defined based on a directional analysis to determine the trajectory direction (between 10 and 16 km) relative to the lidar site. Using the dot product formula, we computed the angle indicating the direction of the trajectory relative to the lidar location. If the angle was less than 90 degrees ($\pi/2$ radians), the trajectory was classified as "Toward lidar or Near", indicating that the balloon was moving in the general direction of the lidar site. If the angle was 90 degrees or more, the trajectory was classified as "Away from OPAR or Far", indicating that the balloon was moving away from the OPAR site (Figure 15). This study was only possible at pseudo-nightly scales, as radiosonde trajectories may be differently classified within the same month. Comparing the Li1200 shift relative to radiosondes for both classes does not reveal a significant effect of horizontal or vertical drift on the relative shift, especially above 13 km (Figure 16). Below 13 km, the lidar wet shift is more evident relative to near radiosondes (Figure 16c), while the overall shift is reduced to approximately 0% when comparing far radiosonde observations (Figure 16a). This is thought to be influenced by ocean effects on radiosonde observations.

Another interpretation is that the Raman lidar may not be significantly affected by fluorescence and, therefore, does not exhibit a wet bias. In this scenario, MLS measurements are genuinely dry in the UT, consistent with previous studies [24,41]. This dry shift in MLS aligns with results from a measurement campaign over Reunion Island in 2013 [26], where, at around 16 km (100 hPa), MLS showed a significant dry shift of 30–40% relative to the lidar. We agree with Dionisi et al. (2015) [26], who suggested that this feature may be caused by both the different instrumental sampling geometries and a systematic bias in MLS within the upper troposphere. This bias is due to its limited vertical resolution across the sharp transition between the dry stratosphere and the moist troposphere [24]. The MLS dry shift might also be related to the influence of clouds. However, the present study assumes collocation with lidar operational times, during which clear skies (with no low or convective clouds) are predominantly observed at night [45]. The potential influence of cirrus clouds on MLS measurements is another aspect that requires further investigation, which the present study does not address.

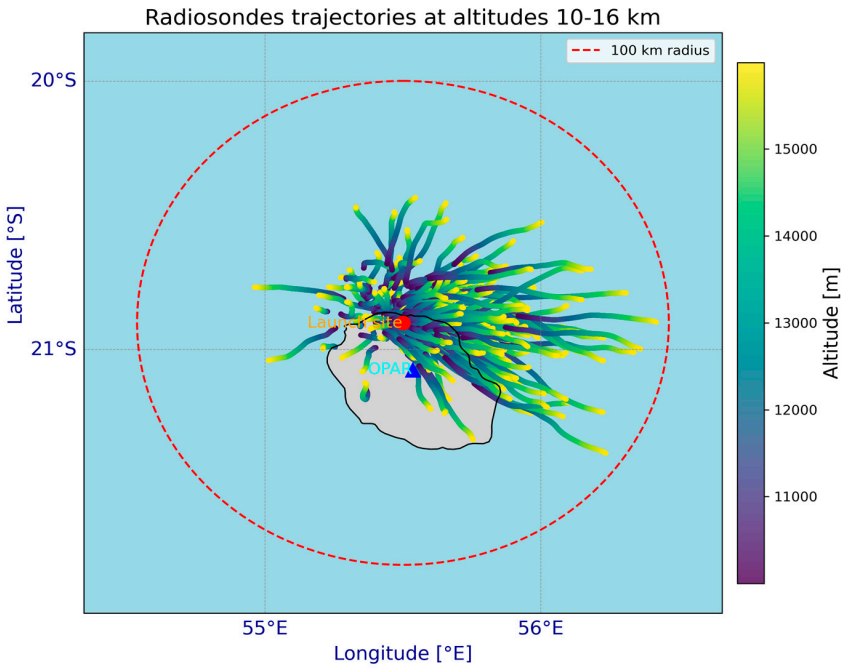

Figure 14. Trajectories of GRUAN M10 radiosondes launched from Saint-Denis airport (red point on Réunion Island) at altitudes between 10 and 16 km. The color of each trajectory represents altitude. The red dashed circle indicates a 100 km radius around the launch site. The blue triangle marks the Maido observatory (Li1200 location).

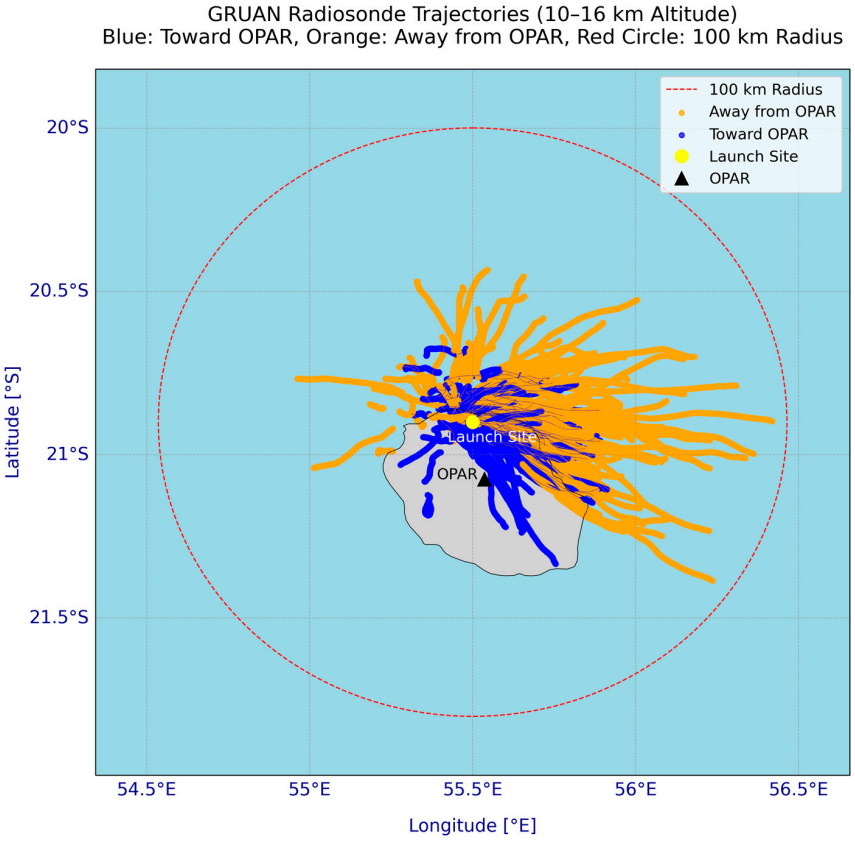

Figure 15. Trajectories of GRUAN M10 radiosondes launched from Saint-Denis airport (yellow point on the Réunion Island) at altitudes between 10 and 16 km. Orange trajectories respresent radiosondes drifts in the opposite direction relative to Li1200 location, classified as 'Far'. Blue trajectories indicates radiosonde drifts towards Li1200 site classified as 'Near'. The red dashed circle indicates a 100 km radius around the launch site. The black triangle marks the Maido observatory (Li1200 location).

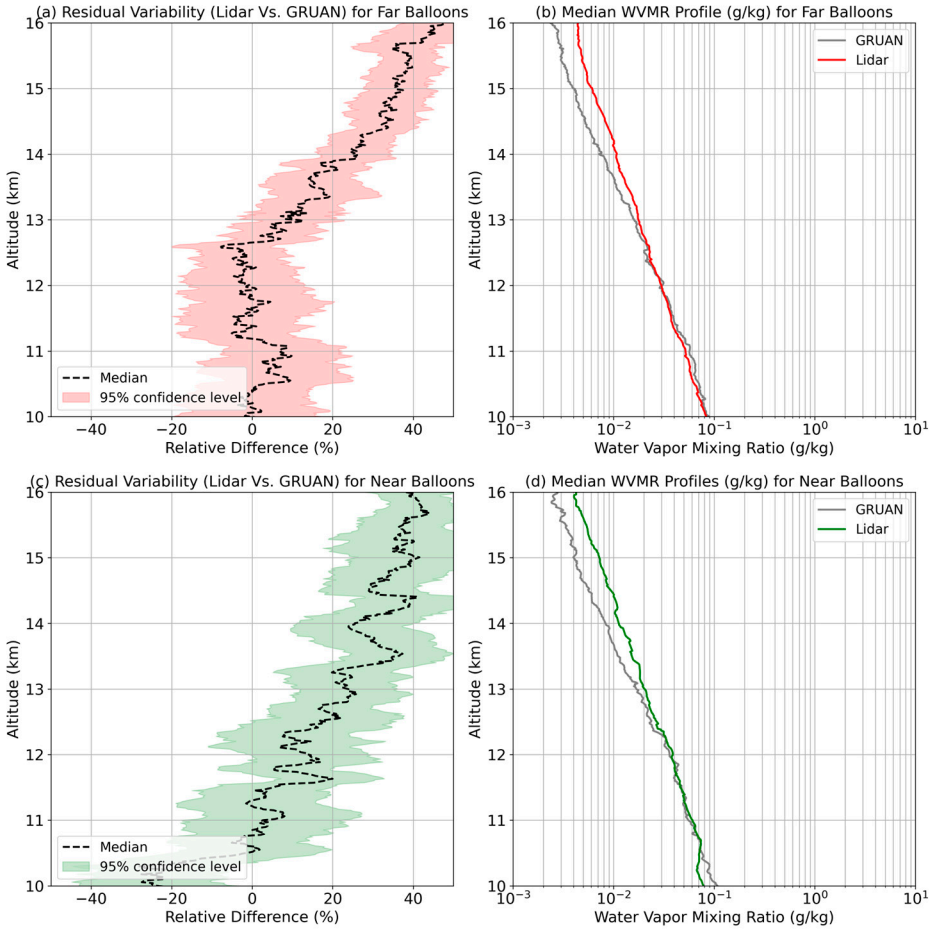

Figure 16. Spatial comparison of Li1200 WVMR relative to GRUAN-processed M10 radiosondes. (**a**) Median relative shift of Li1200 relative to radiosondes drifted far away from the lidar location towards the ocean (%). (**b**) Median WVMR profile (g/kg) for the dates of far drifted radisondes. (**c**) Median relative Li1200 shift (%) relative to near radiosondes. (**d**) Median WVMR profile (g/kg) for dates of radiosondes drifted towards the lidar site (near). Shaded areas indicate the 95% confidence interval of the median relative error.

To our knowledge, GRUAN-processed M10 radiosondes have not been compared to lidar over Reunion Island before. However, previous studies have reported an upper tropospheric dry shift of up to 10% relative to lidar at midlatitudes on finer timescales (hourly) [46]. Measurements by Vaisala RS92 radiosondes have been reported to be drier than those of lidar over midlatitudes [27] and drier than those of Li1200 over the Reunion Island UT during the MALICCA campaign in 2013 [26].

Elevation differences between the GNSS receiver site and the nearest ERA5 grid point over Reunion Island must be considered when evaluating integrated water vapor (IWV), as shown by the study of Lees et al. [47]. They reported differences of up to 12 kg m^{-2} attributable to this elevation mismatch, with ERA5 being wetter than GNSS. The Li1200 dataset, which is calibrated with IWV from GNSS, appears slightly drier than that of ERA5. However, this small shift (5%) in the UT may not necessarily be linked to IWV differences between ERA5 and GNSS.

Given the lidar's operational constraints, the present study is conducted primarily under clear-sky conditions (with no low or convective clouds). Therefore, the parameterization of convective transport schemes in ERA5 is not expected to significantly influence the observed shifts in ERA5. Furthermore, the detected shift in ERA5 is relatively small (within 5%), indicating a strong consistency with the operational lidar dataset over Reunion Island.

On the other hand, multiple studies have reported that ERA5 tends to underestimate relative humidity under ice-supersaturated conditions, which are more frequent at UT altitudes. Comparisons with IAGOS observations confirm that ERA5 generally produces drier relative humidity values with respect to ice at these altitudes [46], leading to several proposed correction approaches [48,49].

However, our current operational Li1200 dataset appears slightly drier than that of ERA5, as demonstrated in Section 3.2, particularly during the dry season. These findings underscore the importance of evaluating the sensitivity of Raman lidar UT retrievals to the calibration methodology. To explore this further, we generated a new lidar WVMR dataset using an alternative calibration method, which is detailed in the following subsection. Most comparisons are subsequently revisited with respect to this new dataset.

4.1. Alternative Li1200 Calibration

In this section, we introduce a novel calibration strategy, building upon the methodology proposed by Alraddawi et al. (2025) [46]. Unlike the conventional approach, which relies on collocated GNSS-derived Integrated Water Vapor (IWV) content as an external calibration reference [30], our method uses the ERA5 reanalysis WVMR product as the calibration reference. Specifically, this method focuses on a narrow altitude band between 4 and 6 km to derive the calibration coefficients. The selection of this altitude range is motivated by prior comparative analyses. By examining ERA5 midnight profiles against GRUAN-processed M10 radiosonde launches over Reunion Island, we identified the 4–6 km layer as the altitude range with the strongest agreement and the smallest bias between the two datasets.

The calibration procedure begins with the construction of lidar-like pseudo-nightly ERA5 profiles. These profiles are extracted from the ERA5 hourly dataset, which is available on 37 pressure levels [20], by selecting only nighttime data that coincide with lidar observations. The resulting pseudo-nightly ERA5 product serves as the external calibration reference.

Following the framework proposed by Alraddawi et al. (2025) [46], nightly calibration factors are first derived and statistically analyzed to identify stable calibration periods. These factors are then generalized and applied to calibrate the entire 2013–2023 lidar nighttime dataset.

The resulting calibration coefficients are comparable in magnitude to those obtained using the conventional GNSS-based approach described by Vérèmes et al. (2019) [30].

Figure 17 presents a comparison between the generalized calibration factors derived using the GNSS-based method [30] and those obtained with the ERA5-based approach [46]. This comparison underscores the overall consistency between the two calibration strategies while offering insights into their respective uncertainties and performance under similar atmospheric conditions.

Using the calibrated nightly dataset, pseudo-monthly profiles are constructed to enable a comparative analysis similar to that presented in Section 3. This newly developed dataset—referred to as Li1200 new in the accompanying figures—is then evaluated alongside established datasets, including ERA5 and GRUAN-processed M10 radiosondes.

Our results indicate that the WVMR datasets remain broadly consistent, regardless of the calibration method applied. However, the Li1200 new dataset exhibits slightly higher WVMR values compared to the operational Li1200 dataset. This difference is illustrated in Figure 18, where the median profiles of both datasets are compared.

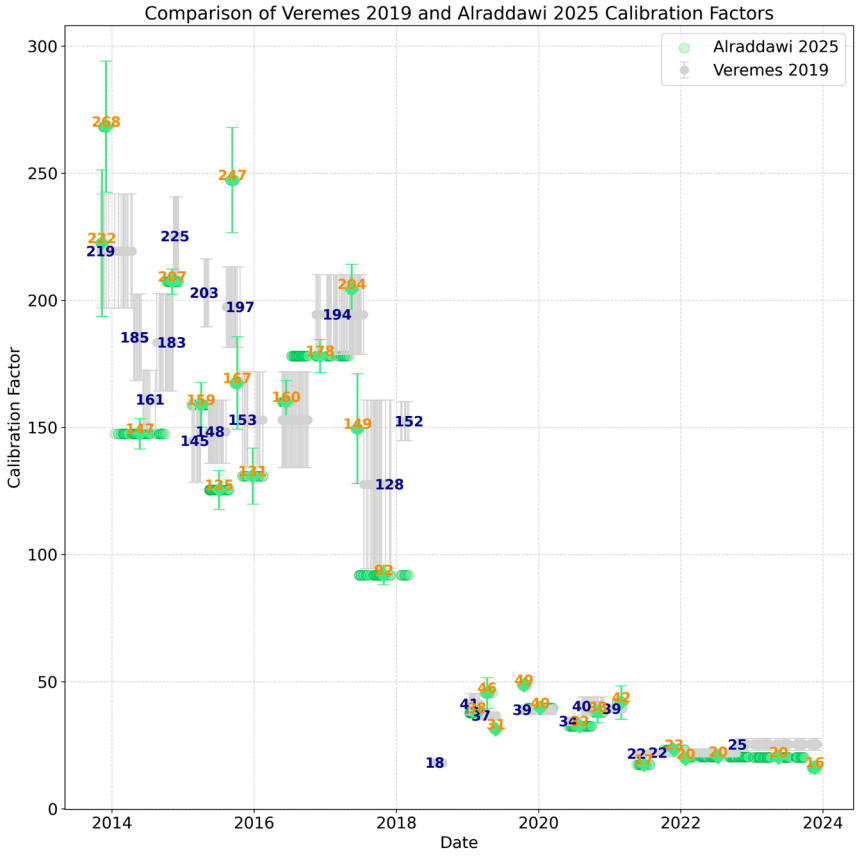

Figure 17. Nightly calibration factors used to derive generalized calibration coefficients over the 2013–2023 period, obtained using the methods of Vérèmes et al. (2019) [30] (gray bars, annotated in dark blue) and Alraddawi et al. (2025) [46] (green bars, annotated in orange). The plot shows the median calibration factors for each stable period, together with their associated uncertainties. Error bars (whiskers) represent the 95% confidence intervals.

Lidar WVMR can be calibrated using a limited portion of a vertically resolved reference profile. In principle, a single-point observation of WVMR at an altitude where the overlap functions are sufficiently well-known and stable can be sufficient for calibration.

The new Li1200 calibration does not rely on total column water vapor, which is dominated by contributions from the lower troposphere. Instead, it uses a limited portion of the ERA5 profile as a reference for calibration. Specifically, the statistical method—similar to that described in [50]—adopted to derive a single calibration factor over several months reduces the influence of individual profile-to-profile variability or specific vertical features of the model. The Li1200 new calibration uses a limited altitude range between 4 and 6 km, chosen because this portion of the ERA5 profile shows the best agreement with GRUAN data and is less influenced by elevation differences between the lidar site and the nearest ERA5 grid point. Moreover, it is important to note that ERA5 is not a profiling instrument. Upper-tropospheric humidity in the model is not necessarily constrained by observations in the same way as in the lower troposphere, where most assimilated data are available. Observing water vapor in the UT using the model remains challenging. Similar studies in tropical and subtropical UT regions, such as the location of the current study, are still rare.

Considering the above perspectives is crucial to avoid circular reasoning and to achieve greater clarity. This approach particularly allows for independent comparisons of the Li1200 new and ERA5 profiles in the upper troposphere, similarly to a previous study conducted over the Parisian region [46].

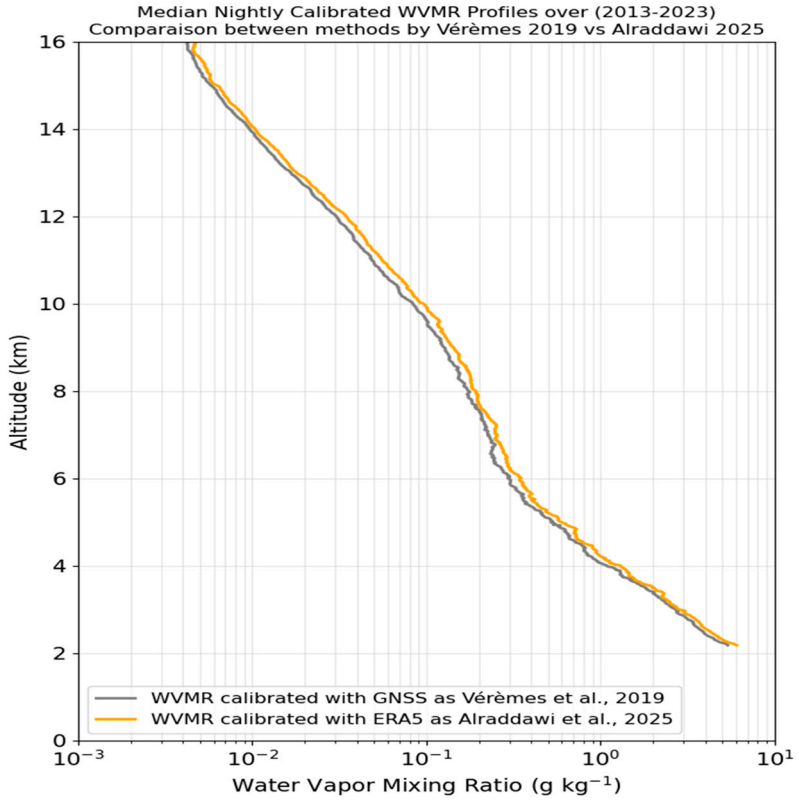

Figure 18. Median WVMR profile (in g/kg) over the 2013–2023 period derived from the two calibration methods: the operational Li1200 dataset calibrated with GNSS IWV [30], and the new alternative ERA5-based calibration [47].

4.2. Li1200-New vs. ERA5

Revisiting Section 3.2, the median shift of the original Li1200 dataset [30] relative to ERA5 did not exceed 5% in the UT, with the lidar being slightly drier than ERA5 at those altitudes (Figure 8). When performing the same comparison using the newly developed dataset 'Li1200 new', we find that the updated lidar profiles are wetter than ERA5 across the entire UT layer (Figure 19). Consequently, a clear dry shift in ERA5 is revealed throughout the UT, reaching up to 20%.

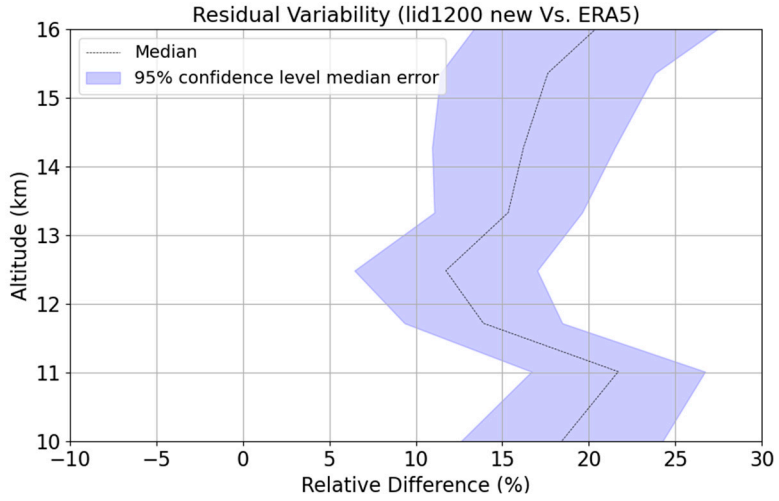

Figure 19. Median relative shift (%) of the Li1200 new dataset relative to ERA5 over the 2013–2023 period. Shaded areas indicate the 95% confidence intervals of the relative error.

An upper tropospheric dry bias in ERA5 over midlatitudes has been reported on numerous occasions, motivating several correction efforts [48,49]. Comparisons with lidar WVMR calibrated similarly to the Li1200 new dataset have shown an ERA5 dry shift of up to 20% relative to lidar in the midlatitude UT region [46]. That study also discussed the potential for partial correction or validation using IAGOS-MOZAIC observations, which, unfortunately, are not available for the southern subtropical site considered in this work.

The seasonal analysis confirms the observed dry shift in ERA5, which reaches up to 20% relative to the Li1200 new lidar dataset. This shift increases with altitude during the dry season (Figure 20c), and can be attributed to the known underestimation of upper tropospheric humidity by ERA5, as discussed earlier in this section. Furthermore, the enhanced calibration applied in the Li1200 new dataset increases the lidar-retrieved water vapor in the UT, resulting in higher values compared to ERA5. This improvement effectively addresses the calibration-related limitations previously observed during the dry season (Figure 10c) with the original calibration method.

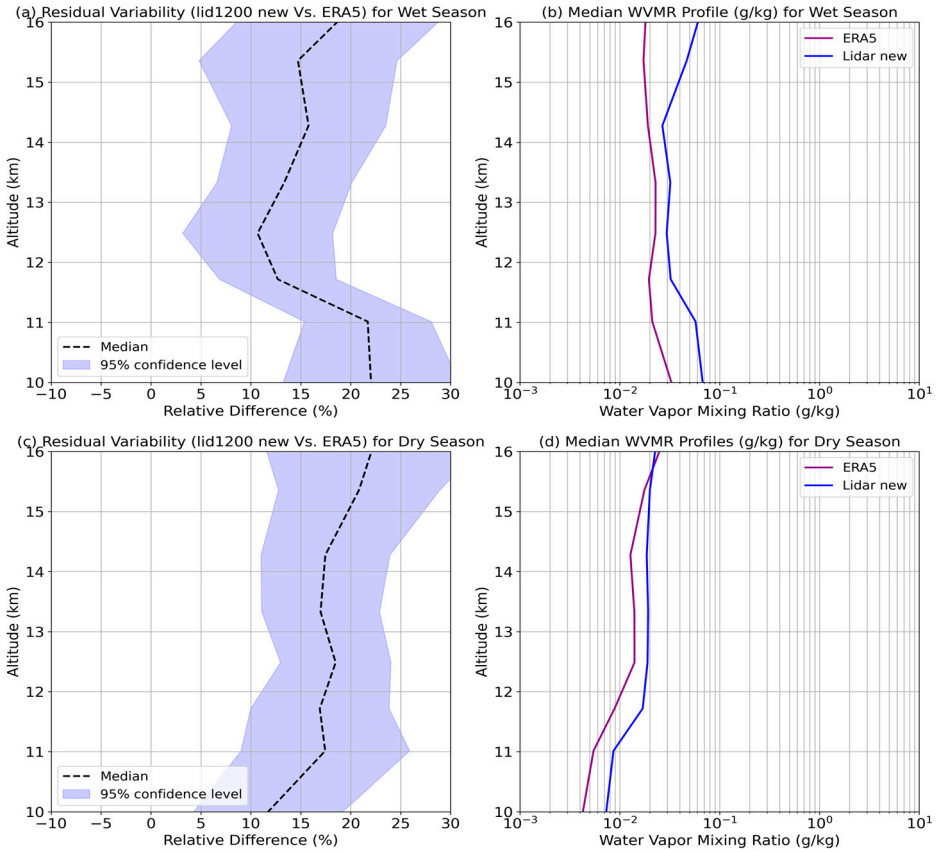

Figure 20. (**a**) Median Li1200 new WVMR relative shift (%) relative to ERA5 during the wet season; (**b**) Median WVMR profile during the wet season (g/kg); (**c**) Median Li1200 new WVMR relative shift (%) relative to ERA5 during the dry season; (**d**) Median WVMR profile during the dry season (g/kg), all over the 2013 to 2023 study period. Shaded areas indicate the 95% confidence intervals of the median error.

4.3. Li1200 New vs. GRUAN-Processed M10

The pseudo-monthly GRUAN-processed M10 dataset exhibits a more pronounced dry shift relative to the Li1200 new dataset across the entire UT altitudes, reaching up to 20% below 13 km and exceeding 40% at higher altitudes (Figure 21). Compared to the operational Li1200 dataset [30], the Li1200 new dataset shows a more pronounced wet shift

relative to the GRUAN-processed M10 dataset across the entire UT. There are almost no altitude layers where Li1200 new is drier than GRUAN, regardless of the season (Figure 22).

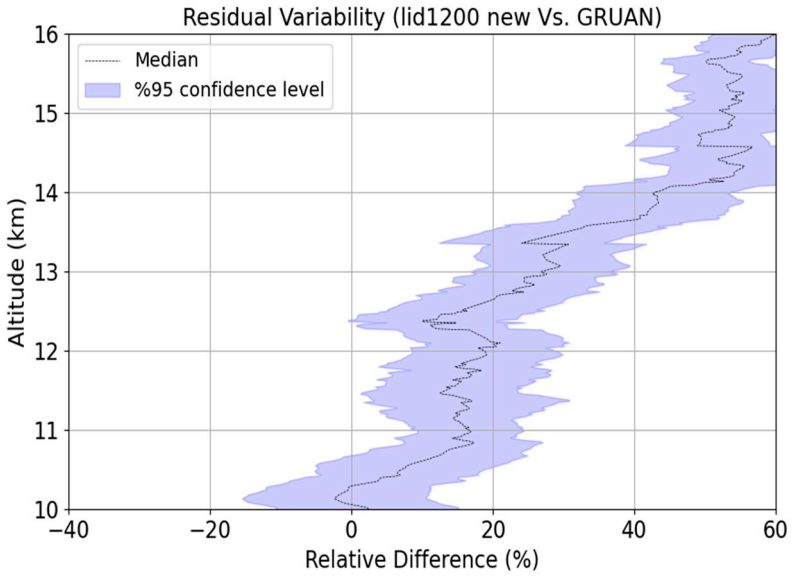

Figure 21. Median relative shift (%) of the Li1200 new WVMR profiles relative to GRUAN-processed M10 radiosondes, based on 41 pseudo-monthly profiles from 2019 to 2023. Shaded areas indicate the 95% confidence intervals of the relative error.

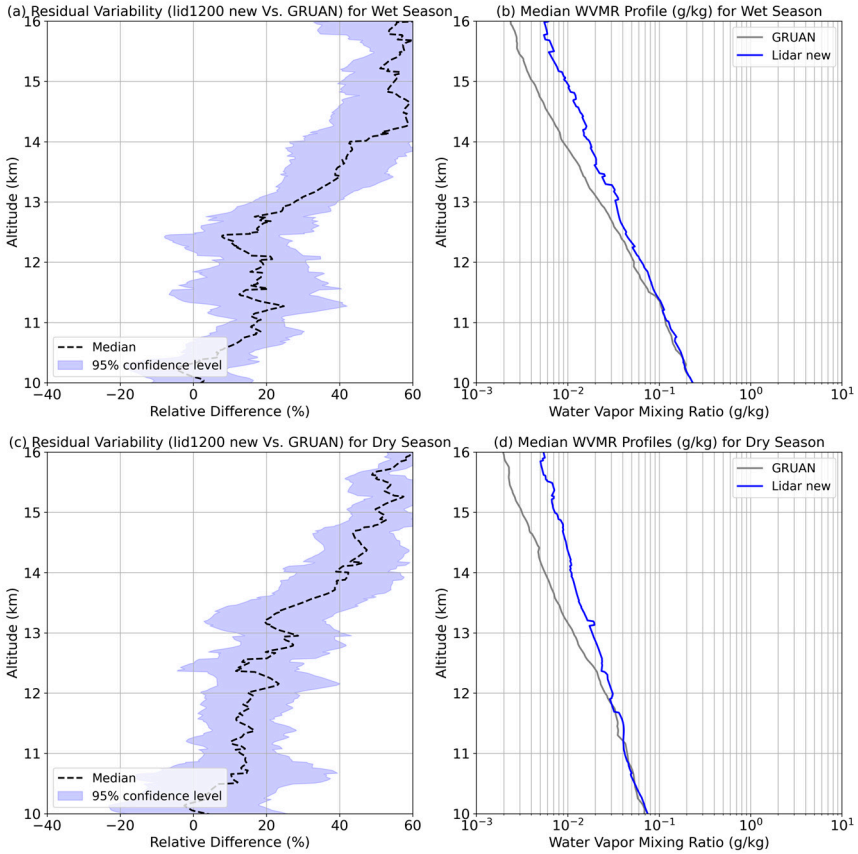

Figure 22. (**a**) Median Li1200 new WVMR relative shift (%) relative to GRUAN-processed M10 radiosondes during the wet season; (**b**) Median WVMR profile during the wet season (g/kg); (**c**) Median Li1200 new WVMR relative shift (%) during the dry season; (**d**) Median WVMR profile during the dry season (g/kg), all over the 2019 to 2023 study period. Shaded areas indicate the 95% confidence intervals of the median error.

This comparison suggests that a portion of the dry shift observed in the operational lidar product relative to GRUAN-processed M10 (Figure 11) may be attributable to the GNSS-based calibration strategy. This strategy can generate lidar WVMR profiles that are drier than reality due to limitations in GNSS reliability at this subtropical site. Previous studies have also reported a dry bias in GNSS measurements over Reunion Island when compared to radiosonde observations [51].

The results of the seasonal analysis at higher UT altitudes (14–16 km), as shown in Figure 22, may be influenced by sampling limitations. In particular, the study period (2019–2023) includes several months with missing data due to factors such as the COVID-19 pandemic and lidar downtimes. Additionally, the number of compared profile pairs decreases with altitude, from 41 pairs at 10 km to only 15 pairs at 16 km. We recommend conducting further analyses over longer periods before drawing conclusions or discussing shifts exceeding 40%.

4.4. Perspectives and Future Horizons

Lidar measurements are inherently constrained by the system's operational requirements, which limit observations to suitable ambient conditions. Consequently, the resulting data are neither continuous nor regularly sampled. In this study, we utilize an 11-year dataset of Raman lidar observations and compare it with the corresponding long-term datasets from MLS and ERA5 at upper-tropospheric altitudes, where observations are already sparse and challenging to obtain.

To address these limitations, we adopted a pseudo-monthly approach as a practical method to enhance the signal-to-noise ratio while maximizing the use of available lidar observations. However, this approach is still constrained by reduced sampling. For instance, in the MLS/lidar comparison, the pseudo-monthly scaling is applied only when at least three lidar-like MLS overpasses occur within a given month. As a result, months with insufficient sampling are excluded from the analysis.

Additionally, due to the observational constraints of lidar, the effective sample size decreases with altitude. For this reason, the analysis is limited to altitudes up to 16 km, as most pseudo-monthly lidar profiles extend to this altitude. For example, in the MLS/lidar comparison, the number of profile pairs ranges from 76 at 10 km to 73 at 16 km.

Generally, the achieved spatiotemporal coincidence is sufficient for these comparisons, as all datasets are subject to strictly similar sampling. However, the representativeness of pseudo-monthly datasets—including ERA5—could be questioned for trend studies. Future work will focus on assessing the sensitivity of trend analyses derived from lidar, lidar-like MLS, ERA5, and GRUAN-processed M10 pseudo-monthly datasets. These will be compared with full nocturnal monthly datasets from MLS and ERA5 to evaluate whether the current dataset can be reliably used for meaningful climatological studies.

The Li1200 new WVMR dataset has provided a valuable long-term record of upper tropospheric humidity since 2013. In line with GRUAN requirements, developing alternative and universal calibration methods is essential to maintain the dataset under quality control and to help detect and investigate potential anomalies in the lidar system.

Many of the perspectives discussed above could be further explored in future measurement campaigns planned over Reunion Island. These campaigns would allow further testing of the impact of different calibration strategies and improving the spatial and temporal collocation with GRUAN-processed radiosondes. This study lays the groundwork for such investigations by providing a comprehensive statistical analysis and by highlighting open questions regarding lidar calibration, dataset shifts, and intercomparisons with satellite and reanalysis data.

The analytical method presented here could be applied to other lidar systems and sites. It would be particularly valuable to implement similar systems with comparable performance at multiple subtropical sites, especially in light of the upcoming deployment of satellites designed to measure water vapor in the UTLS.

5. Conclusions

Valuable information on upper tropospheric humidity can be obtained globally from satellites such as MLS, from reanalysis products like ECMWF-ERA5, and locally from radiosondes (GRUAN) and Raman lidar. However, accurate measurements of WVMR in the UT remain challenging, particularly in less studied subtropical regions.

In this study, we analyzed and statistically compared 11 years of WVMR profiles—derived from these diverse datasets—over Reunion Island for the period 2013–2023. A pseudo-monthly screening approach was applied to the lidar observations to enhance the signal-to-noise ratio and extend WVMR retrievals into the subtropical UT. This approach also mitigates the limited number of collocated MLS overpasses at finer temporal scales. A consistent comparison methodology was applied across all datasets to ensure robust and reliable results.

The multi-dataset comparison at a pseudo-monthly scale reveals the following key results:

1 MLS: A pronounced dry shift relative to lidar is observed, reaching up to 30% in the upper troposphere, particularly above 12 km and during the wet season. This dry bias aligns with previous studies [26,41], which also reported significant underestimation of upper-tropospheric WVMR by MLS compared to lidar.

2 ERA5: ERA5 shows better overall agreement with lidar. However, the operational Li1200 dataset [30] exhibits a small dry shift relative to ERA5, generally below 5% and up to 10% during the dry season. When using the newly calibrated Li1200 new dataset [47], ERA5 demonstrates a clear dry shift of up to 20% in the upper troposphere, particularly above 14 km. Similar dry biases in ERA5 have been previously reported over midlatitude regions [46,48,49].

3 GRUAN-processed M10 radiosondes: GRUAN-processed M10 radiosondes exhibit a pronounced dry shift relative to Li1200, particularly above 13 km. This shift does not appear to be affected by potential mismatches due to radiosonde drift, which can reach up to 100 km from the launch site. Below 13 km, lidar measurements are slightly drier, by 5–10%. This bias may be partially caused by the GNSS-based calibration, as GNSS-derived IWV measurements over Reunion Island have been previously reported to be drier than radiosonde measurements [51]. This hypothesis could further explain why no dry shift in lidar relative to GRUAN-processed M10 radiosondes is observed when comparing the Li1200 new dataset, which is calibrated using a different method.

In conclusion, the pseudo-monthly screening approach has enhanced the capacity of the Raman lidar technique to characterize WVMR in the subtropical upper troposphere. The results demonstrate magnitudes comparable to those derived from MLS, ERA5, and GRUAN-processed M10 datasets, regardless of the calibration strategy employed.

An alternative, universal calibration method offers the advantage of maintaining the lidar dataset under rigorous quality control, while also aiding in the detection and investigation of potential anomalies within the lidar system.

An upcoming measurement campaign could further refine and extend this analysis to a broader range of atmospheric conditions, such as the presence of cirrus clouds, over this important subtropical region.

This 11-year comparative record provides a foundation for future work. Especially, it will enable the assessment of the sensitivity of trend analyses derived from lidar, lidar-like MLS, ERA5, and GRUAN pseudo-monthly datasets. These analyses can then be compared with the full nocturnal monthly datasets from MLS, ERA5, and GRUAN. Such comparisons will help determine whether the current pseudo-monthly lidar dataset can be reliably used for meaningful climatological studies.

Author Contributions: Conceptualization, P.K.; methodology, D.A. and A.H.; software, G.P. and H.V.; validation, P.K. and D.A.; formal analysis, D.A.; investigation, D.A., A.H. and M.S.; resources, P.K.; data curation, D.A. and G.P.; writing—original draft preparation, D.A.; writing—review and editing, J.-L.B., F.M., A.H., A.I. and A.S.; visualization, D.A.; supervision, P.K.; project administration, P.K.; funding acquisition, P.K. All authors have read and agreed to the published version of the manuscript.

Funding: This project has received funding from the Horizon Europe Research and Innovation Actions program under Grant Agreement N°101056885 through the BeCoM (Better Contrail Mitigation) project and from the French government (BPI) in the frame of France 2030 under Grant DOS0182433/00 for the CONTRAILS project.

Data Availability Statement: ERA5 datasets are publicly available at: https://cds.climate.copernicus.eu/datasets/reanalysis-era5-pressure-levels?tab=download, last accessed on 25 March 2026; the GRUAN-analyzed M10 radiosondes dataset is from the IPSL climserv data server. MLS data are publicly available at: https://acdisc.gesdisc.eosdis.nasa.gov/data/Aura_MLS_Level2/ML2H2O.005/, last accessed on 11 February 2026.

Acknowledgments: The authors would like to thank the technical and IT staff of the Li1200 lidar. The authors would like to thank also Milena Martic (Grodien Strato co.) for the lidar expertise. This work was partly funded by the European Union under grant agreement No 101086690 and by the COST Action EARLICOST (CA24135), supported by COST (European Cooperation in Science and Technology). The authors acknowledge the support of the ANR through the OBS4CLIM project (ANR-21-ESRE-0013), and CNES through the projects EarthCARE, AOS, and EXTRASAT. The authors also acknowledge the support of OPAR (Observatoire de Physique de l'Atmosphère à la Réunion) and OSU-Réunion (Observatoire des Sciences de l'Univers à La Réunion, UAR 3365), funded by CNRS (INSU), Météo-France, and Université de La Reunion.

Conflicts of Interest: The authors declare no conflicts of interest.

References

1. Qian, L.; Rao, J.; Ren, R.; Shi, C.; Liu, S. Enhanced stratosphere-troposphere and tropics-Arctic couplings in the 2023/24 winter. *Commun. Earth Environ.* **2024**, *5*, 631. [CrossRef]
2. Gettelman, A.; Fu, Q. Observed and Simulated Upper-Tropospheric Water Vapor Feedback. *J. Clim.* **2008**, *21*, 3282–3289. [CrossRef]
3. Dessler, A.E.; Zhang, Z.; Yang, P. Water-vapor climate feedback inferred from climate fluctuations, 2003–2008. *Geophys. Res. Lett.* **2008**, *35*, 2008GL035333. [CrossRef]
4. Colman, R.; Soden, B.J. Water vapor and lapse rate feedbacks in the climate system. *Rev. Mod. Phys.* **2021**, *93*, 045002. [CrossRef]
5. Wang, X.; Dessler, A.E. The response of stratospheric water vapor to climate change driven by different forcing agents. *Atmos. Chem. Phys.* **2020**, *20*, 13267–13282. [CrossRef]
6. Wulfmeyer, V.; Hardesty, R.M.; Turner, D.D.; Behrendt, A.; Cadeddu, M.P.; Di Girolamo, P.; Schlüssel, P.; Van Baelen, J.; Zus, F. A review of the remote sensing of lower tropospheric thermodynamic profiles and its indispensable role for the understanding and the simulation of water and energy cycles. *Rev. Geophys.* **2015**, *53*, 819–895. [CrossRef]
7. Kämpfer, N. *Monitoring Atmospheric Water Vapour: Ground-Based Remote Sensing and In-Situ Methods*; Springer Science & Business Media: Berlin/Heidelberg, Germany, 2012; Volume 10.
8. Fetzer, E.J.; Read, W.G.; Waliser, D.; Kahn, B.H.; Tian, B.; Vömel, H.; Irion, F.W.; Su, H.; Eldering, A.; Juarez, M.d.l.T.; et al. Comparison of upper tropospheric water vapor observations from the Microwave Limb Sounder and Atmospheric Infrared Sounder. *J. Geophys. Res. Atmos.* **2008**, *113*, 2008JD010000. [CrossRef]

9. Read, W.G.; Lambert, A.; Bacmeister, J.; Cofield, R.E.; Christensen, L.E.; Cuddy, D.T.; Daffer, W.H.; Drouin, B.J.; Fetzer, E.; Froidevaux, L.; et al. Aura Microwave Limb Sounder upper tropospheric and lower stratospheric H_2O and relative humidity with respect to ice validation. *J. Geophys. Res. Atmos.* **2007**, *112*, 2007JD008752. [CrossRef]
10. Read, W.G.; Stiller, G.; Lossow, S.; Kiefer, M.; Khosrawi, F.; Hurst, D.; Vömel, H.; Rosenlof, K.; Dinelli, B.M.; Raspollini, P.; et al. The SPARC Water Vapor Assessment II: Assessment of satellite measurements of upper tropospheric humidity. *Atmos. Meas. Tech.* **2022**, *15*, 3377–3400. [CrossRef]
11. Waters, J.W.; Froidevaux, L.; Harwood, R.S.; Jarnot, R.F.; Pickett, H.M.; Read, W.G.; Siegel, P.H.; Cofield, R.E.; Filipiak, M.J.; Flower, D.; et al. The earth observing system microwave limb sounder (EOS MLS) on the aura satellite. *IEEE Trans. Geosci. Remote Sens.* **2006**, *44*, 1075–1092. [CrossRef]
12. Davis, S.M.; Damadeo, R.; Flittner, D.; Rosenlof, K.H.; Park, M.; Randel, W.J.; Hall, E.G.; Huber, D.; Hurst, D.F.; Jordan, A.F.; et al. Validation of SAGE III/ISS Solar Water Vapor Data with Correlative Satellite and Balloon-Borne Measurements. *J. Geophys. Res. Atmos.* **2021**, *126*, e2020JD033803. [CrossRef]
13. Hegglin, M.I.; Tegtmeier, S.; Anderson, J.; Froidevaux, L.; Fuller, R.; Funke, B.; Jones, A.; Lingenfelser, G.; Lumpe, J.; Pendlebury, D.; et al. SPARC Data Initiative: Comparison of water vapor climatologies from international satellite limb sounders. *J. Geophys. Res. Atmos.* **2013**, *118*, 11824–11846. [CrossRef]
14. Vömel, H.; David, D.E.; Smith, K. Accuracy of tropospheric and stratospheric water vapor measurements by the cryogenic frost point hygrometer: Instrumental details and observations. *J. Geophys. Res.* **2007**, *112*, 2006JD007224. [CrossRef]
15. Vömel, H.; Naebert, T.; Dirksen, R.; Sommer, M. An update on the uncertainties of water vapor measurements using cryogenic frost point hygrometers. *Atmos. Meas. Tech.* **2016**, *9*, 3755–3768. [CrossRef]
16. Fujiwara, M.; Vömel, H.; Hasebe, F.; Shiotani, M.; Ogino, S.; Iwasaki, S.; Nishi, N.; Shibata, T.; Shimizu, K.; Nishimoto, E.; et al. Seasonal to decadal variations of water vapor in the tropical lower stratosphere observed with balloon-borne cryogenic frost point hygrometers. *J. Geophys. Res.* **2010**, *115*, 2010JD014179. [CrossRef]
17. Dirksen, R.J.; Bodeker, G.E.; Thorne, P.W.; Merlone, A.; Reale, T.; Wang, J.; Hurst, D.F.; Demoz, B.B.; Gardiner, T.D.; Ingleby, B.; et al. Managing the transition from Vaisala RS92 to RS41 radiosondes within the Global Climate Observing System Reference Upper-Air Network (GRUAN): A progress report. *Geosci. Instrum. Methods Data Syst.* **2020**, *9*, 337–355. [CrossRef]
18. Sperber, D.; Gierens, K. Towards a more reliable forecast of ice supersaturation: Concept of a one-moment ice-cloud scheme that avoids saturation adjustment. *Atmos. Chem. Phys.* **2023**, *23*, 15609–15627. [CrossRef]
19. Hersbach, H.; Bell, B.; Berrisford, P.; Hirahara, S.; Horányi, A.; Muñoz-Sabater, J.; Nicolas, J.; Peubey, C.; Radu, R.; Schepers, D.; et al. The ERA5 global reanalysis. *Q. J. R. Meteorol. Soc.* **2020**, *146*, 1999–2049. [CrossRef]
20. Hersbach, H.; Bell, B.; Berrisford, P.; Biavati, G.; Horányi, A.; Muñoz Sabater, J.; Nicolas, J.; Peubey, C.; Radu, R.; Rozum, I.; et al. *ERA5-Hourly Data on Model Levels*; [Data Set]; ECMWF: Reading, UK, 2023.
21. Konjari, P.; Rolf, C.; Hegglin, M.I.; Rohs, S.; Li, Y.; Zahn, A.; Bönisch, H.; Nedelec, P.; Krämer, M.; Petzold, A. Technical note: Water vapour climatologies in the extra-tropical upper troposphere and lower stratosphere derived from a synthesis of passenger and research aircraft measurements. *Atmos. Meas. Tech.* **2025**, *25*, 4269–4289. [CrossRef]
22. Mazière, M.D.; Thompson, A.M.; Kurylo, M.J.; Wild, J.D.; Bernhard, G.; Blumenstock, T.; Braathen, G.O.; Hannigan, J.W.; Lambert, J.C.; Leblanc, T.; et al. The Network for the Detection of Atmospheric Composition Change (NDACC): History, status and perspectives. *Atmos. Chem. Phys.* **2018**, *18*, 4935–4964. [CrossRef]
23. Klanner, L.; Höveler, K.; Khordakova, D.; Perfahl, M.; Rolf, C.; Trickl, T.; Vogelmann, H. A powerful lidar system capable of 1 h measurements of water vapour in the troposphere and the lower stratosphere as well as the temperature in the upper stratosphere and mesosphere. *Atmos. Meas. Tech.* **2021**, *14*, 531–555. [CrossRef]
24. Leblanc, T.; McDermid, I.; Walsh, T. Ground-based water vapor Raman lidar measurements up to the upper troposphere and lower stratosphere for long-term monitoring. *Atmos. Meas. Tech.* **2012**, *5*, 17–36. [CrossRef]
25. Whiteman, D.N.; Rush, K.; Rabenhorst, S.; Welch, W.; Cadirola, M.; McIntire, G.; Russo, F.; Adam, M.; Venable, D.; Connell, R.; et al. Airborne and Ground-Based Measurements Using a High-Performance Raman Lidar. *J. Atmos. Ocean. Technol.* **2010**, *27*, 1781–1801. [CrossRef]
26. Dionisi, D.; Keckhut, P.; Courcoux, Y.; Hauchecorne, A.; Porteneuve, J.; Baray, J.L.; de Bellevue, J.L.; Vérèmes, H.; Gabarrot, F.; Payen, G.; et al. Water vapor observations up to the lower stratosphere through the Raman lidar during the Maïdo Lidar Calibration Campaign. *Atmos. Meas. Tech.* **2015**, *8*, 1425–1445. [CrossRef]
27. Bock, O.; Bosser, P.; Bourcy, T.; David, L.; Goutail, F.; Hoareau, C.; Keckhut, P.; Legain, D.; Pazmino, A.; Pelon, J.; et al. Accuracy assessment of water vapour measurements from in-situ and remote sensing techniques during the DEMEVAP 2011 campaign at OHP. *Atmos. Meas. Tech. Discuss.* **2013**, *6*, 2777–2802. [CrossRef]
28. Baray, J.-L.; Courcoux, Y.; Keckhut, P.; Portafaix, T.; Tulet, P.; Cammas, J.-P.; Hauchecorne, A.; Godin-Beekmann, S.; De Mazière, M.; Hermans, C.; et al. Maïdo observatory: A new high-altitude station facility at Reunion Island (21° S, 55° E) for long-term atmospheric remote sensing and in situ measurements. *Atmos. Meas. Tech.* **2013**, *6*, 2865–2877. [CrossRef]

29. Keckhut, P.; Courcoux, Y.; Baray, J.-L.; Porteneuve, J.; Vérèmes, H.; Hauchecorne, A.; Dionisi, D.; Posny, F.; Cammas, J.-P.; Payen, G.; et al. Introduction to the Maïdo Lidar Calibration Campaign dedicated to the validation of upper air meteorological parameters. *J. Appl. Remote Sens.* **2015**, *9*, 094099. [CrossRef]
30. Vérèmes, H.; Payen, G.; Keckhut, P.; Duflot, V.; Baray, J.-L.; Cammas, J.-P.; Evan, S.; Posny, F.; Körner, S.; Bosser, P. Validation of the Water Vapor Profiles of the Raman Lidar at the Maïdo Observatory (Reunion Island) Calibrated with Global Navigation Satellite System Integrated Water Vapor. *Atmosphere* **2019**, *10*, 713. [CrossRef]
31. Sherlock, V.; Garnier, A.; Hauchecorne, A.; Keckhut, P. Implementation and validation of a Raman lidar measurement of middle and upper tropospheric water vapor. *Appl. Opt.* **1999**, *38*, 5838–5850. [CrossRef]
32. Keckhut, P.; Chanin, M.-L.; Hauchecorne, A. Stratosphere temperature measurement using Raman lidar. *Appl. Opt.* **1990**, *29*, 5182–5186. [CrossRef]
33. Emardson, T.R.; Derks, H.J.P. On the relation between the wet delay and the integrated precipitable water vapour in the European atmosphere. *Meteorol. Appl.* **2000**, *7*, 61–68. [CrossRef]
34. Ning, T.; Wang, J.; Elgered, G.; Dick, G.; Wickert, J.; Bradke, M.; Sommer, M.; Querel, R.; Smale, D. The uncertainty of the atmospheric integrated water vapour estimated from GNSS observations. *Atmos. Meas. Tech.* **2016**, *9*, 79–92. [CrossRef]
35. Leblanc, T.; Sica, R.J.; van Gijsel, J.A.E.; Godin-Beekmann, S.; Haefele, A.; Trickl, T.; Payen, G.; Gabarrot, F. Proposed standardized definitions for vertical resolution and uncertainty in the NDACC lidar ozone and temperature algorithms—Part 1: Vertical resolution. *Atmos. Meas. Tech.* **2016**, *9*, 4029–4049. [CrossRef]
36. Livesey, N.J.; Van Snyder, W.; Read, W.G.; Wagner, P.A. Retrieval algorithms for the EOS Microwave limb sounder (MLS). *IEEE Trans. Geosci. Remote Sens.* **2006**, *44*, 1144–1155. [CrossRef]
37. Lambert, A.; Read, W.G.; Livesey, N.J.; Santee, M.L.; Manney, G.L.; Froidevaux, L.; Wu, D.L.; Schwartz, M.J.; Pumphrey, H.C.; Jimenez, C.; et al. Validation of the Aura Microwave Limb Sounder middle atmosphere water vapor and nitrous oxide measurements. *J. Geophys. Res.* **2007**, *112*, 2007JD008724. [CrossRef]
38. Vömel, H.; Barnes, J.E.; Forno, R.N.; Fujiwara, M.; Hasebe, F.; Iwasaki, S.; Kivi, R.; Komala, N.; Kyrö, E.; Leblanc, T.; et al. Validation of Aura Microwave Limb Sounder water vapor by balloon-borne Cryogenic Frost point Hygrometer measurements. *J. Geophys. Res.* **2007**, *112*, 2007JD008698. [CrossRef]
39. Berthet, G.; Renard, J.-B.; Ghysels, M.; Durry, G.; Gaubicher, B.; Amarouche, N. Balloon-borne observations of mid-latitude stratospheric water vapour: Comparisons with HALOE and MLS satellite data. *J. Atmos. Chem.* **2013**, *70*, 197–219. [CrossRef]
40. Hurst, D.F.; Lambert, A.; Read, W.G.; Davis, S.M.; Rosenlof, K.H.; Hall, E.G.; Jordan, A.F.; Oltmans, S.J. Validation of Aura Microwave Limb Sounder stratospheric water vapor measurements by the NOAA frost point hygrometer. *J. Geophys. Res. Atmos.* **2014**, *119*, 1612–1625. [CrossRef]
41. Yan, X.; Wright, J.S.; Zheng, X.; Livesey, N.J.; Vömel, H.; Zhou, X. Validation of Aura MLS retrievals of temperature, water vapour and ozone in the upper troposphere and lower–middle stratosphere over the Tibetan Plateau during boreal summer. *Atmos. Meas. Tech.* **2016**, *9*, 3547–3566. [CrossRef]
42. Seidel, D.J.; Berger, F.H.; Diamond, H.J.; Dykema, J.; Goodrich, D.; Immler, F.; Murray, W.; Peterson, T.; Sisterson, D.; Sommer, M.; et al. Reference Upper-Air Observations for Climate: Rationale, Progress, and Plans. *Bull. Am. Meteorol. Soc.* **2009**, *90*, 361–369. [CrossRef]
43. Dupont, J.-C.; Haeffelin, M.; Badosa, J.; Clain, G.; Raux, C.; Vignelles, D. Characterization and corrections of relative humidity measurement from Meteomodem M10 radiosondes at midlatitude stations. *J. Atmos. Ocean. Technol.* **2020**, *37*, 857–871. [CrossRef]
44. Chouza, F.; Leblanc, T.; Brewer, M.; Wang, P.; Martucci, G.; Haefele, A.; Vérèmes, H.; Duflot, V.; Payen, G.; Keckhut, P. The impact of aerosol fluorescence on long-term water vapor monitoring by Raman lidar and evaluation of a potential correction method. *Atmos. Meas. Tech.* **2022**, *15*, 4241–4256. [CrossRef]
45. Durand, J.; Lees, E.; Bousquet, O.; Delanoë, J.; Bonnardot, F. Cloud Radar Observations of Diurnal and Seasonal Cloudiness over Reunion Island. *Atmosphere* **2021**, *12*, 868. [CrossRef]
46. Alraddawi, D.; Keckhut, P.; Mandija, F.; Sarkissian, A.; Pietras, C.; Dupont, J.-C.; Farah, A.; Hauchecorne, A.; Porteneuve, J. Calibration of Upper Air Water Vapour Profiles Using the IPRAL Raman Lidar and ERA5 Model Results and Comparison to GRUAN Radiosonde Observations. *Atmosphere* **2025**, *16*, 351. [CrossRef]
47. Lees, E.; Bousquet, O.; Roy, D.; Bellevue, J.L.D. Analysis of diurnal to seasonal variability of Integrated Water Vapour in the South Indian Ocean basin using ground-based GNSS and fifth-generation ECMWF reanalysis (ERA5) data. *Q. J. R. Meteorol. Soc.* **2020**, *147*, 229–248. [CrossRef]
48. Hofer, S.; Gierens, K.; Rohs, S. How well can persistent contrails be predicted? An update. *Atmos. Chem. Phys.* **2024**, *24*, 7911–7925. [CrossRef]
49. Wolf, K.; Bellouin, N.; Boucher, O.; Rohs, S.; Li, Y. Correction of temperature and relative humidity biases in ERA5 by bivariate quantile mapping: Implications for contrail classification. *EGUsphere* **2023**, *preprint*. [CrossRef]

50. Hoareau, C.; Keckhut, P.; Sarkissian, A.; Baray, J.-L.; Durry, G. Methodology for water monitoring in the upper troposphere with Raman lidar at the Haute-Provence Observatory. *J. Atmos. Ocean. Technol.* **2009**, *26*, 2149–2160. [CrossRef]
51. Bosser, P.; Van Baelen, J.; Bousquet, O. Routine Measurement of Water Vapour Using GNSS in the Framework of the Map-Io Project. *Atmosphere* **2022**, *13*, 903. [CrossRef]